$k_{Ar}^{\Delta J}$ for NaK $2(A)^1\Sigma^+(v=16, J=30)$

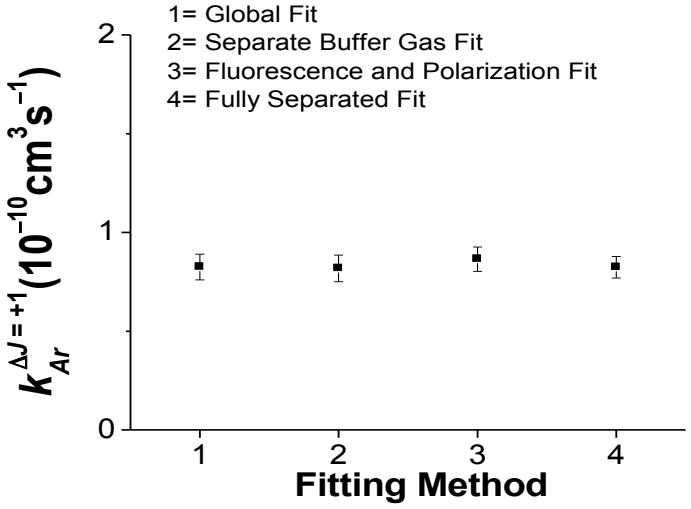

(a) $\Delta J = +1$

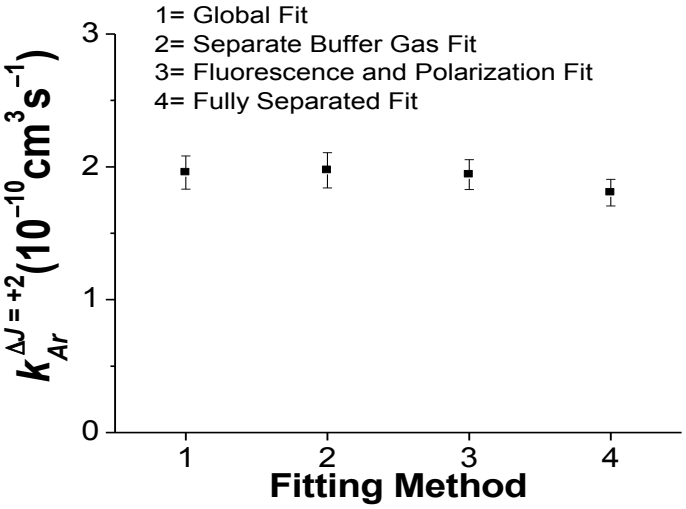

(b) $\Delta J = +2$

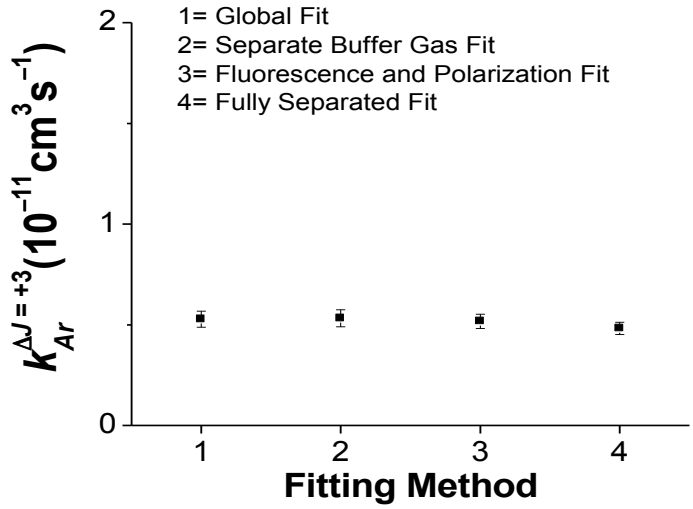

(c) $\Delta J = +3$

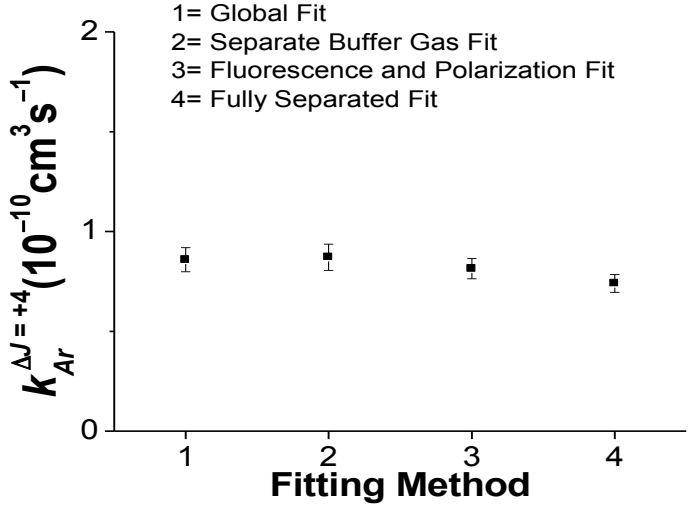

(d) $\Delta J = +4$

Supplementary Material Fig. 1a: Plots of the fitted argon J-changing rate coefficients $k_{Ar}^{\Delta J}$ following excitation of NaK molecules to the $2(A)^1\Sigma^+(v=16, J=30)$ level, for each of the fitting methods described in the text ($+4 \geq \Delta J \geq +1$).

$k_{Ar}^{\Delta J}$ for NaK $2(A)^1\Sigma^+(v=16, J=30)$

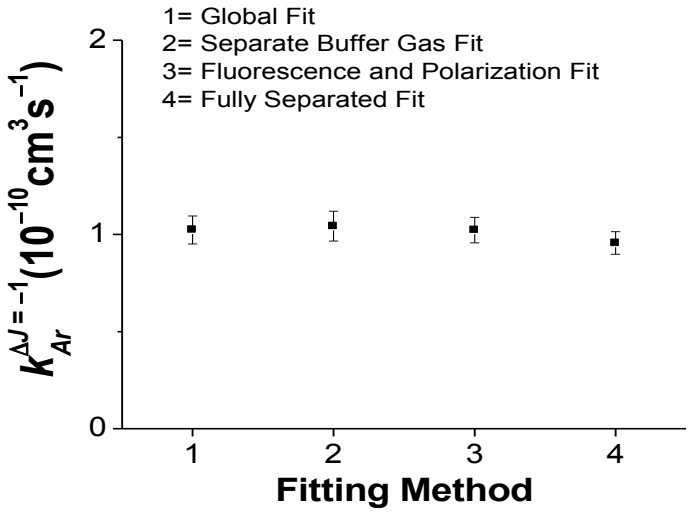

(a) $\Delta J = -1$

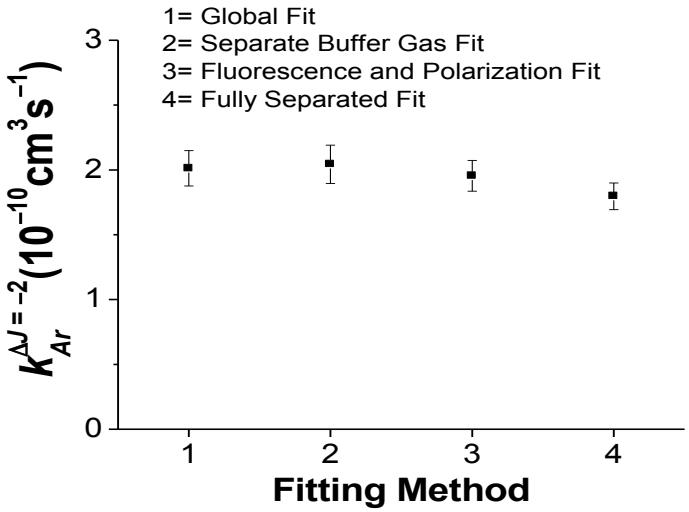

(b) $\Delta J = -2$

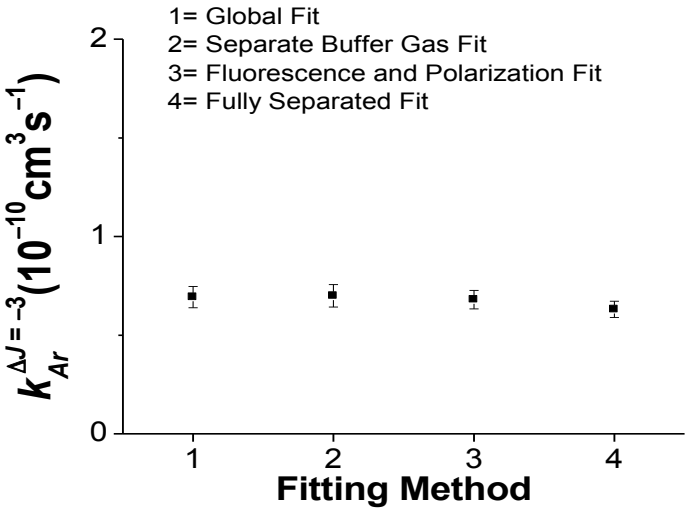

(c) $\Delta J = -3$

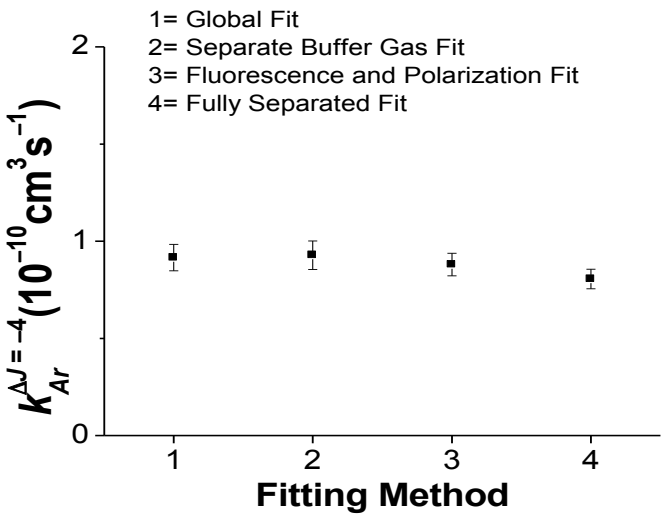

(d) $\Delta J = -4$

Supplementary Material Fig. 1b: Plots of the fitted argon J-changing rate coefficients $k_{Ar}^{\Delta J}$ following excitation of NaK molecules to the $2(A)^1\Sigma^+(v=16, J=30)$ level, for each of the fitting methods described in the text ($-4 \le \Delta J \le -1$).

$k_{He}^{\Delta J}$ for NaK $2(A)^1\Sigma^+(v=16, J=30)$

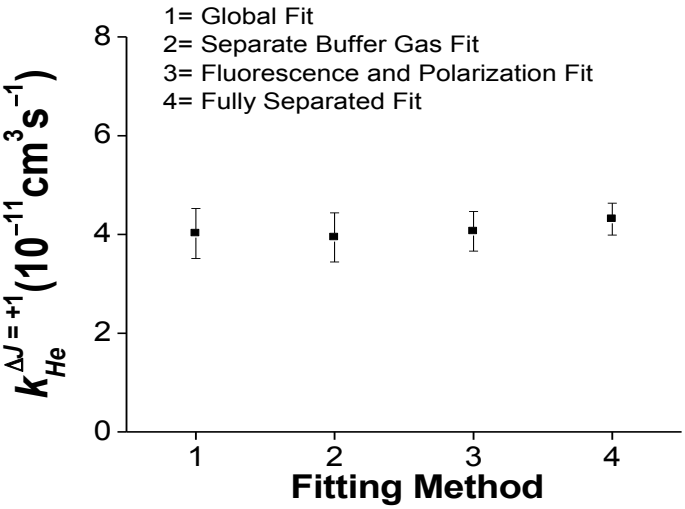

(a) $\Delta J = +1$

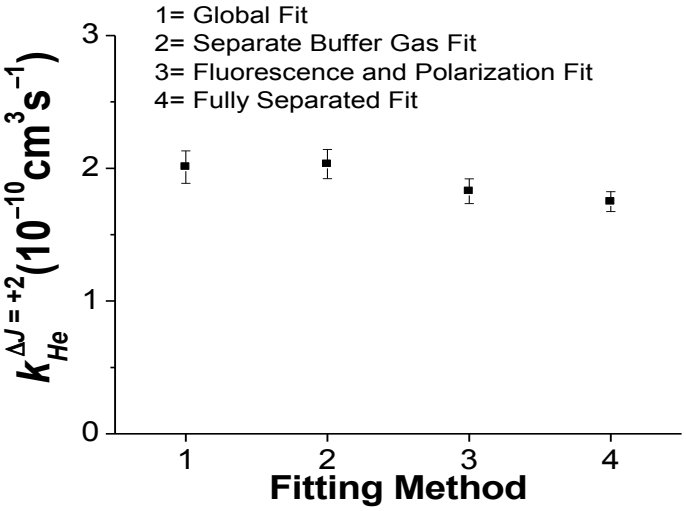

(b) $\Delta J = +2$

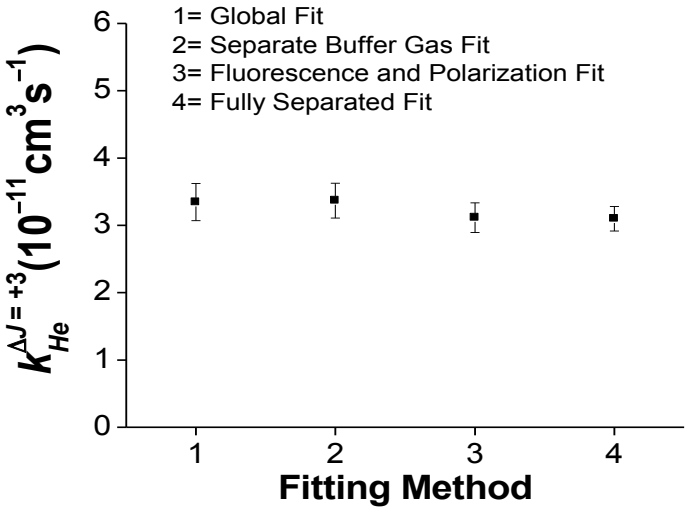

(c) $\Delta J = +3$

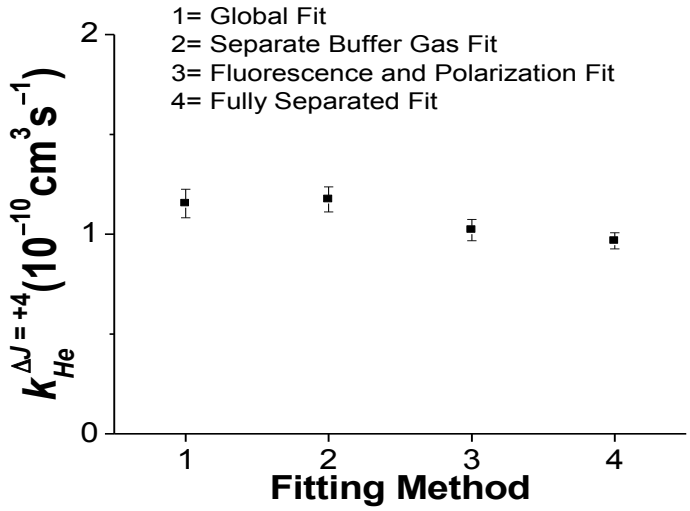

(d) $\Delta J = +4$

Supplementary Material Fig. 2a: Plots of the fitted helium J-changing rate coefficients $k_{He}^{\Delta J}$ following excitation of NaK molecules to the $2(A)^1\Sigma^+(v=16, J=30)$ level, for each of the fitting methods described in the text ($+4 \geq \Delta J \geq +1$).

$k_{He}^{\Delta J}$ for NaK $2(A)^1\Sigma^+(v=16, J=30)$

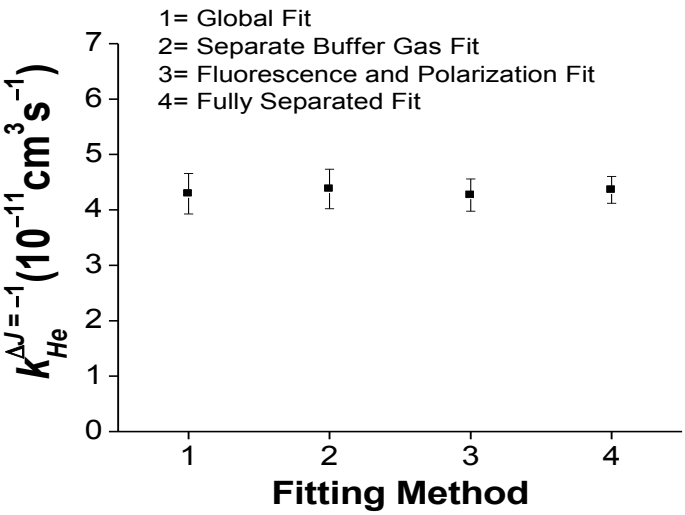

(a) $\Delta J = -1$

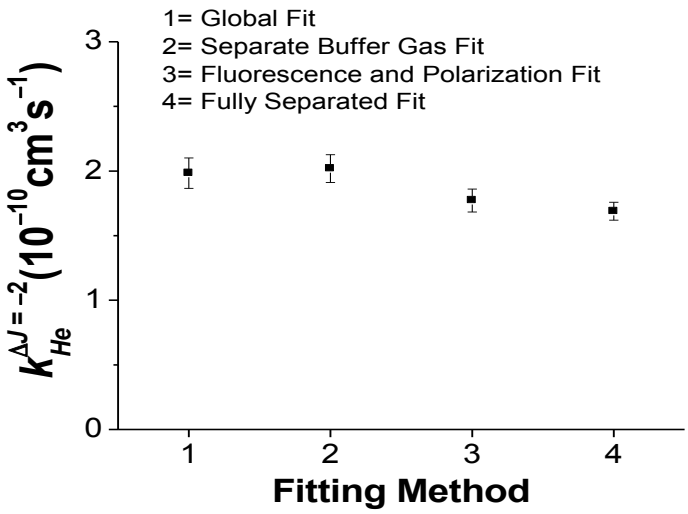

(b) $\Delta J = -2$

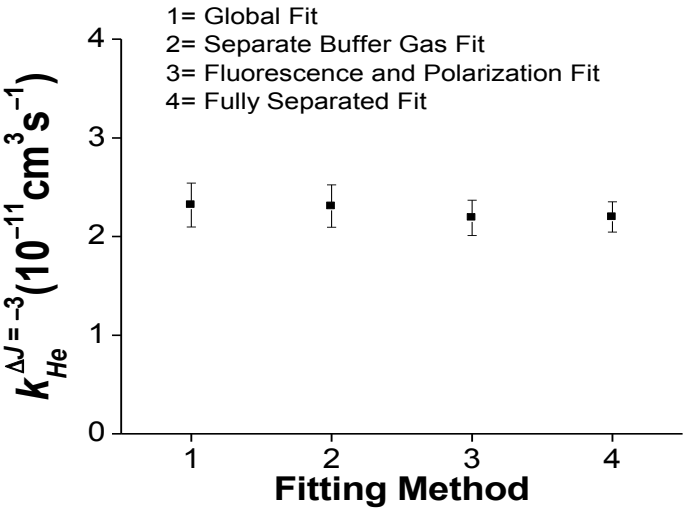

(c) $\Delta J = -3$

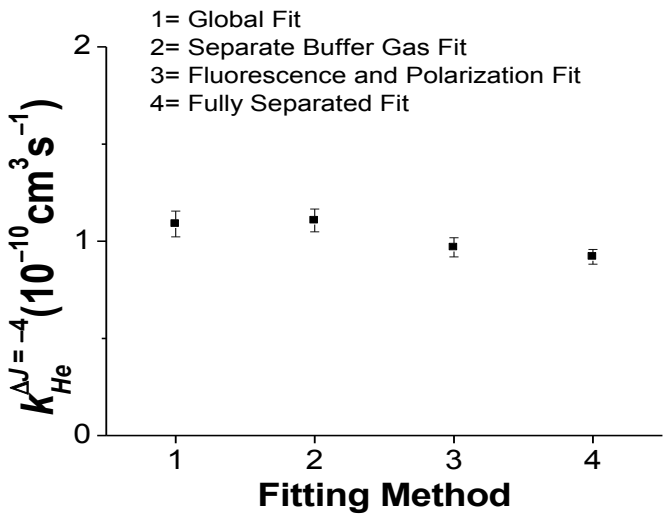

(d) $\Delta J = -4$

Supplementary Material Fig. 2b: Plots of the fitted helium J-changing rate coefficients $k_{He}^{\Delta J}$ following excitation of NaK molecules to the $2(A)^1\Sigma^+(v=16, J=30)$ level, for each of the fitting methods described in the text ($-4 \le \Delta J \le -1$).

$k_K^{\Delta J}$ for NaK $2(A)^1\Sigma^+(v=16, J=30)$

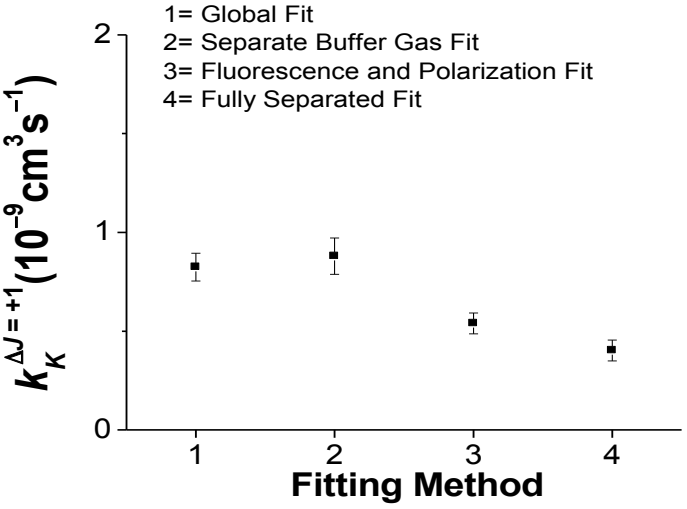

(a) $\Delta J = +1$

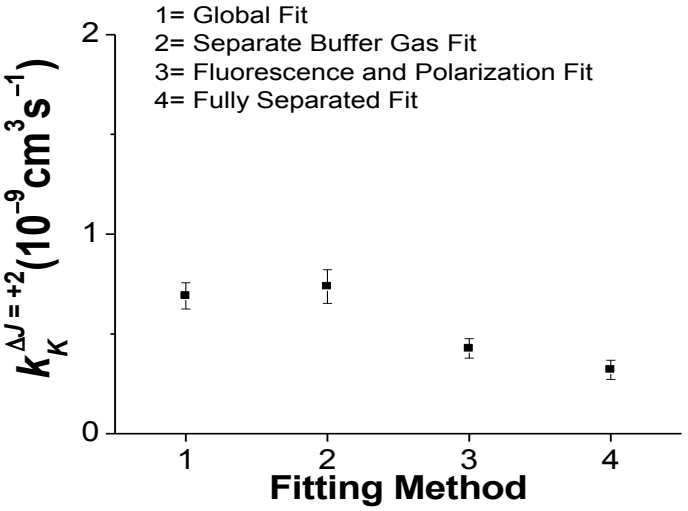

(b) $\Delta J = +2$

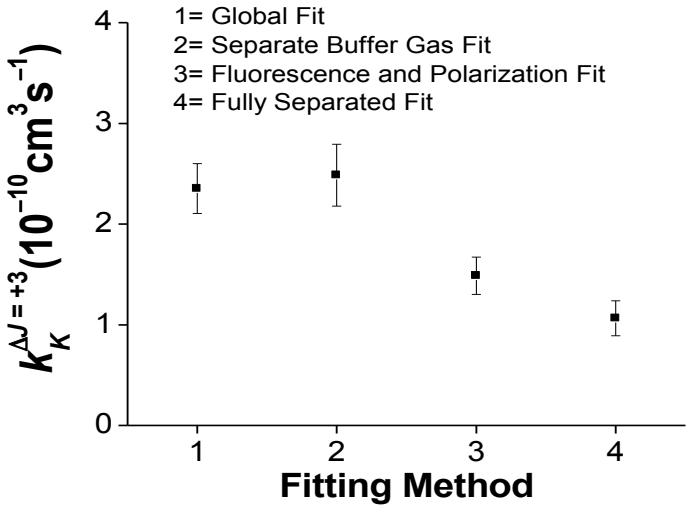

(c) $\Delta J = +3$

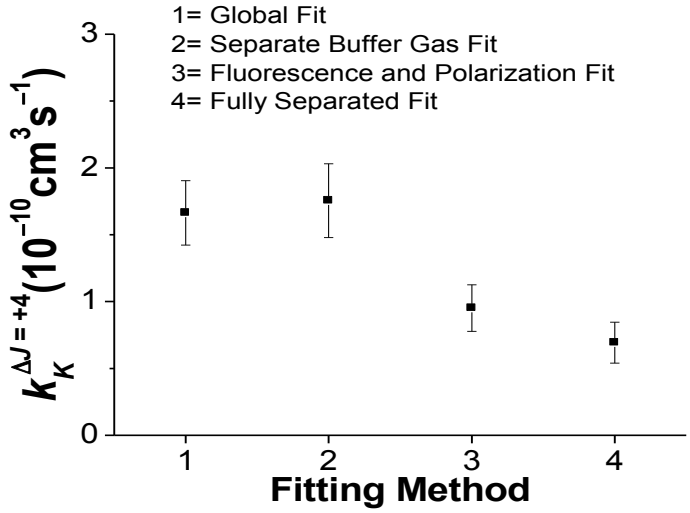

(d) $\Delta J = +4$

Supplementary Material Fig. 3a: Plots of the fitted potassium *J*-changing rate coefficients $k_K^{\Delta J}$ following excitation of NaK molecules to the $2(A)^1\Sigma^+(v=16, J=30)$ level, for each of the fitting methods described in the text ($+4 \geq \Delta J \geq +1$).

$k_K^{\Delta J}$ for NaK $2(A)^1\Sigma^+(v=16, J=30)$

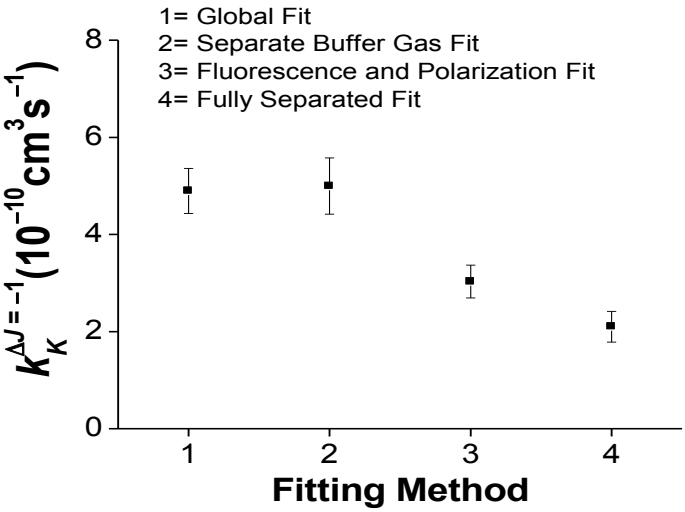

(a) $\Delta J = -1$

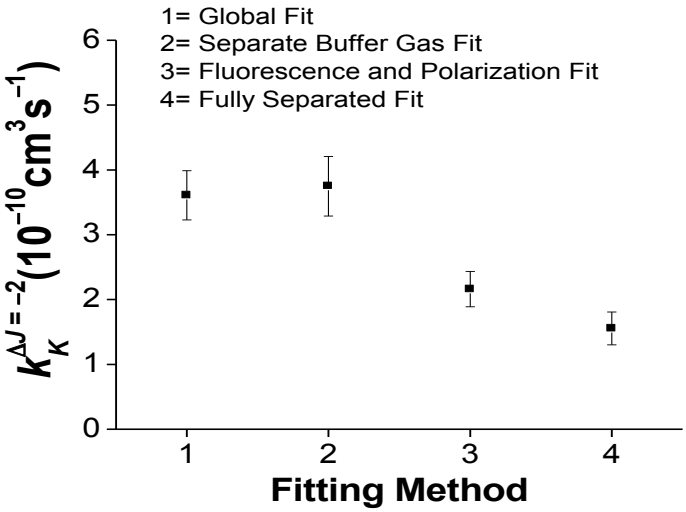

(b) $\Delta J = -2$

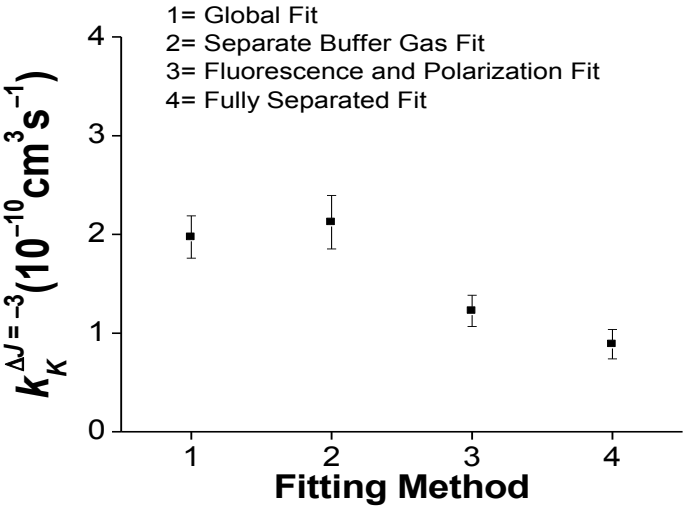

(c) $\Delta J = -3$

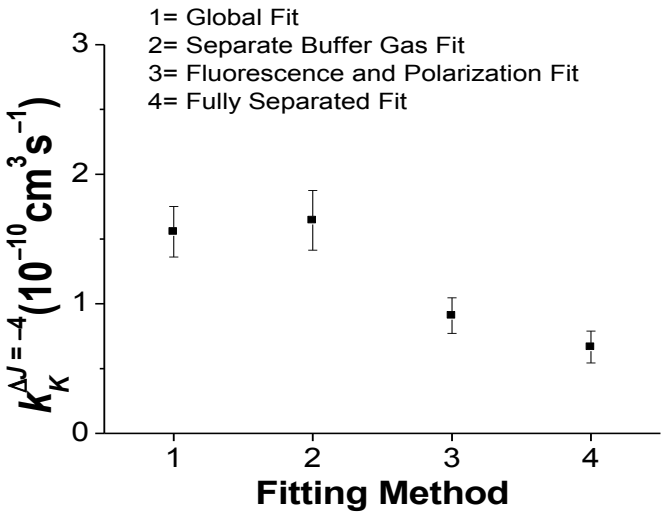

(d) $\Delta J = -4$

Supplementary Material Fig. 3b: Plots of the fitted potassium J-changing rate coefficients $k_K^{\Delta J}$ following excitation of NaK molecules to the $2(A)^1\Sigma^+(v=16, J=30)$ level, for each of the fitting methods described in the text ($-4 \le \Delta J \le -1$).

k_p^Q for NaK $2(A)^1\Sigma^+(v=16, J=30)$

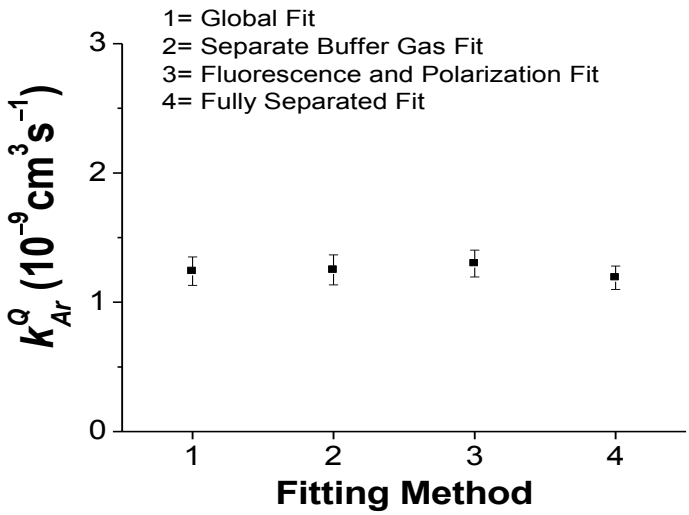

(a) k_{Ar}^Q

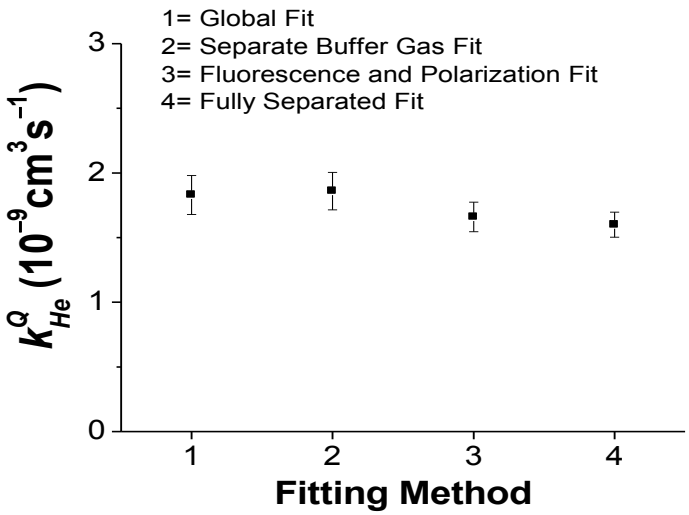

(b) k_{He}^Q

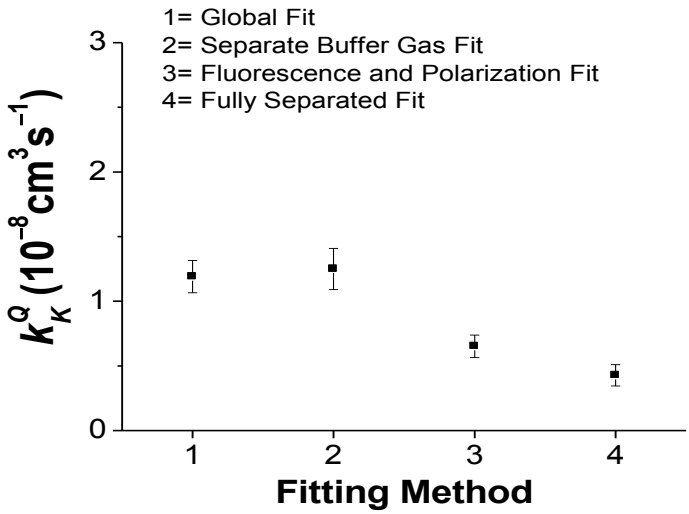

(c) k_K^Q

Supplementary Material Fig. 4: Plots of the fitted quenching rate coefficients k_p^Q following excitation of NaK molecules to the $2(A)^1\Sigma^+(v=16, J=30)$ level, for each of the fitting methods described in the text. a) argon, b) helium, and c) potassium collisions.

$f_{Ar}^{\Delta J}$ for NaK $2(A)^1\Sigma^+(v=16, J=30)$

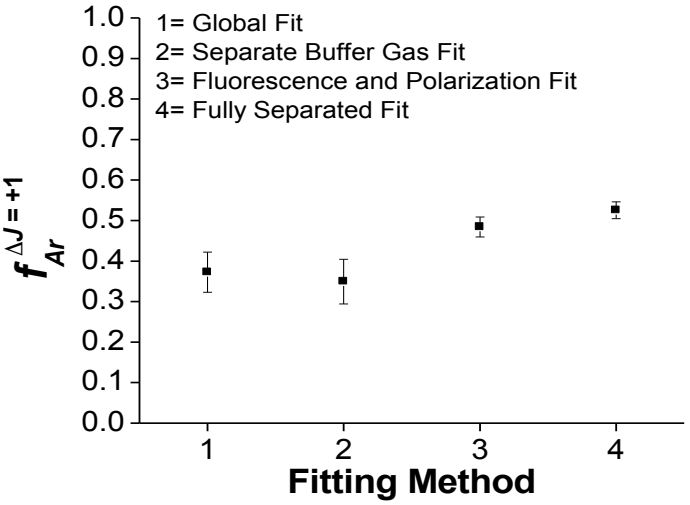

(a) $\Delta J = +1$

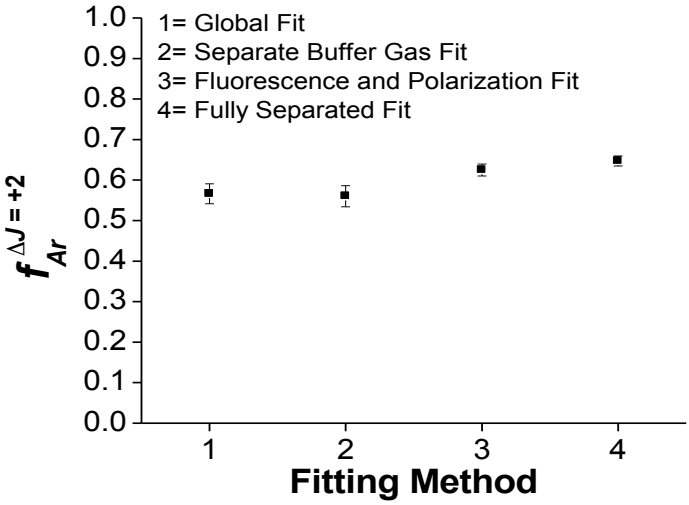

(b) $\Delta J = +2$

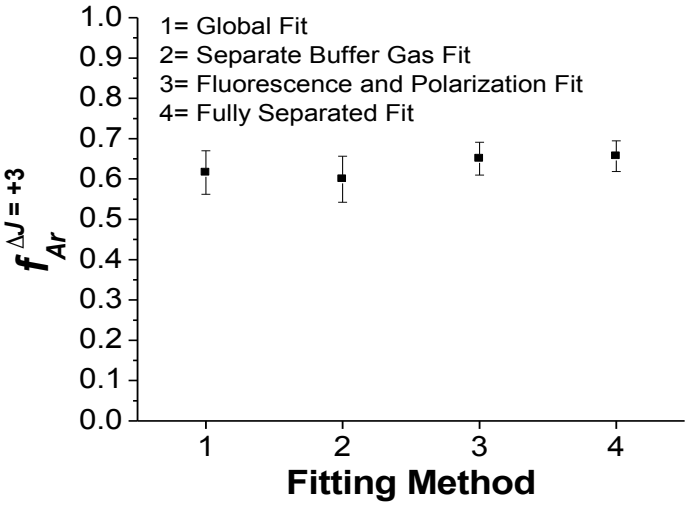

(c) $\Delta J = +3$

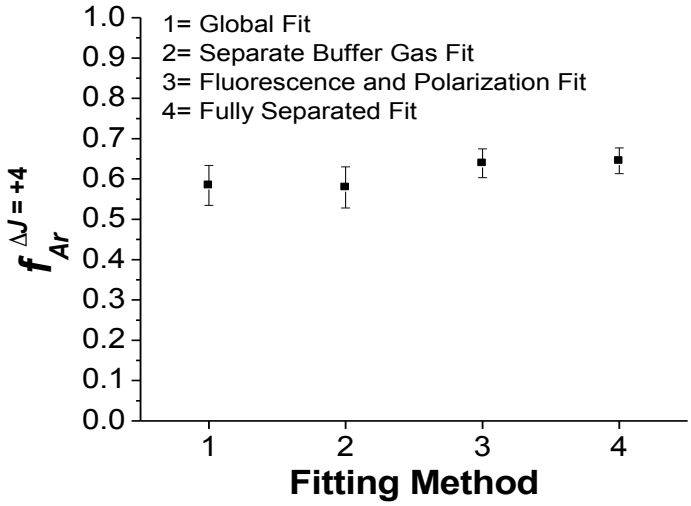

(d) $\Delta J = +4$

Supplementary Material Fig. 5a: Plots of the fitted fraction of orientation destroyed $f_{Ar}^{\Delta J}$ for argon collisions following excitation of NaK molecules to the $2(A)^1\Sigma^+(v=16, J=30)$ level, for each of the fitting methods described in the text ($+4 \geq \Delta J \geq +1$).

$f_{Ar}^{\Delta J}$ for NaK $2(A)^1\Sigma^+(v=16, J=30)$

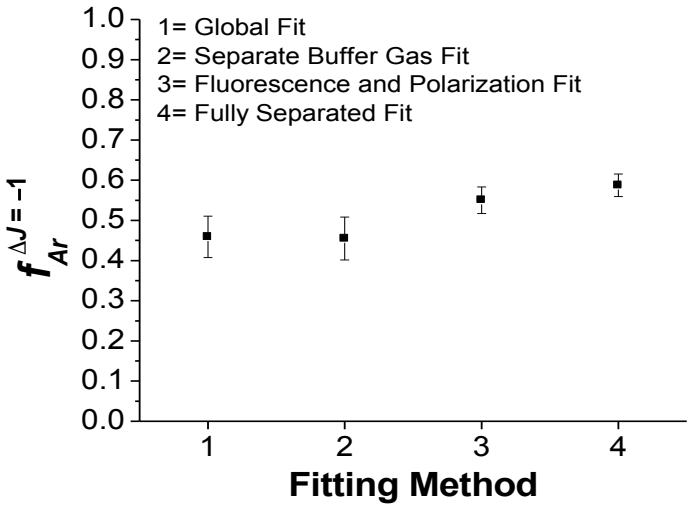

(a) $\Delta J = -1$

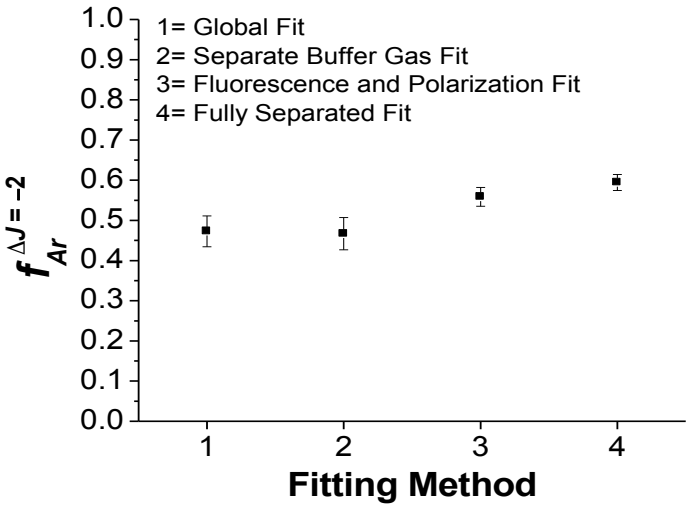

(b) $\Delta J = -2$

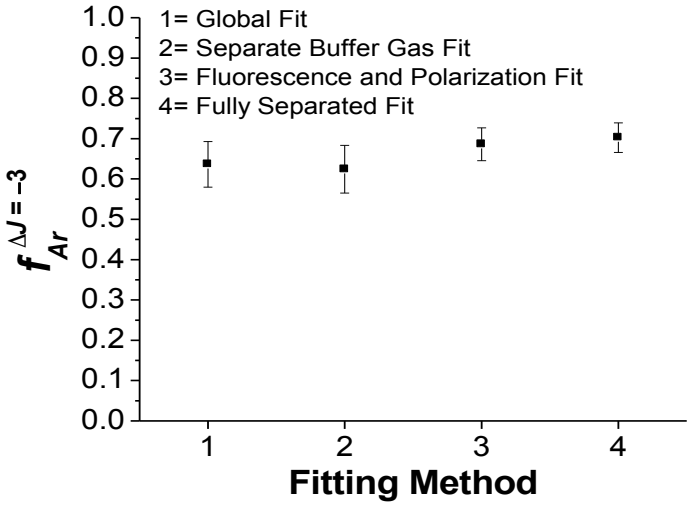

(c) $\Delta J = -3$

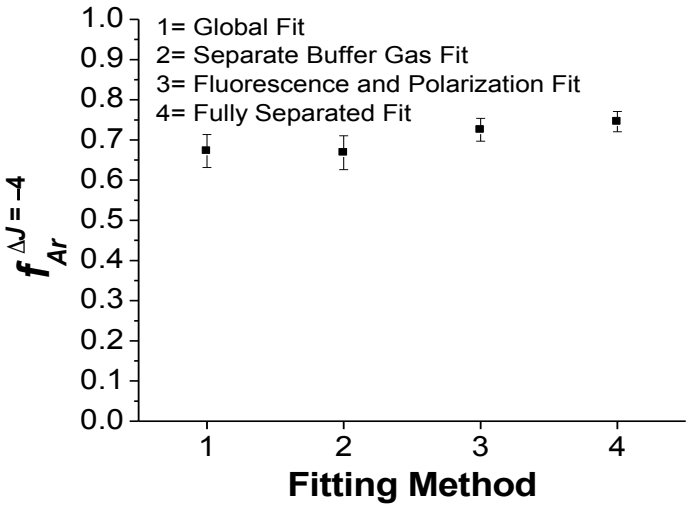

(d) $\Delta J = -4$

Supplementary Material Fig. 5b: Plots of the fitted fraction of orientation destroyed $f_{Ar}^{\Delta J}$ for argon collisions following excitation of NaK molecules to the $2(A)^1\Sigma^+(v=16, J=30)$ level, for each of the fitting methods described in the text ($-4 \le \Delta J \le -1$).

$f_{He}^{\Delta J}$ for NaK $2(A)^1\Sigma^+(v=16, J=30)$

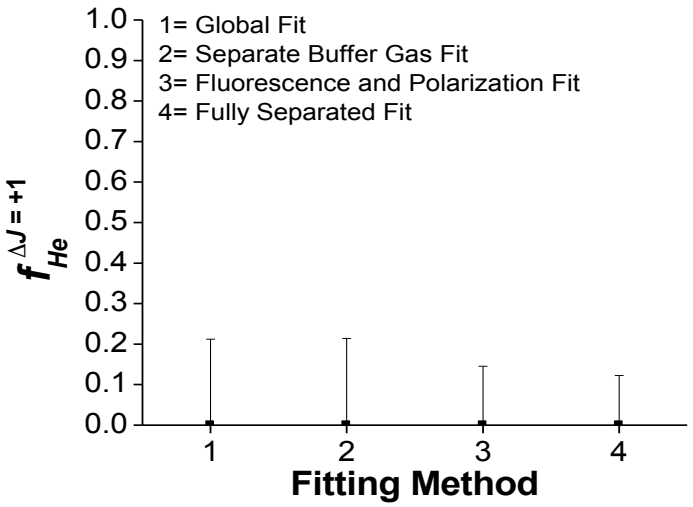

(a) $\Delta J = +1$

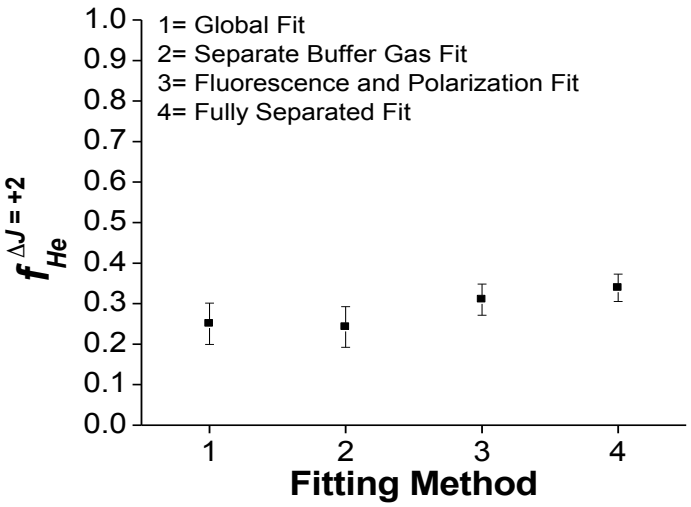

(b) $\Delta J = +2$

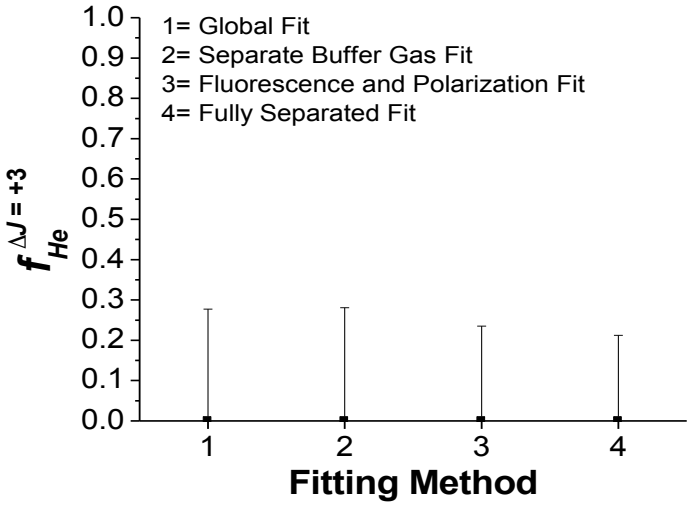

(c) $\Delta J = +3$

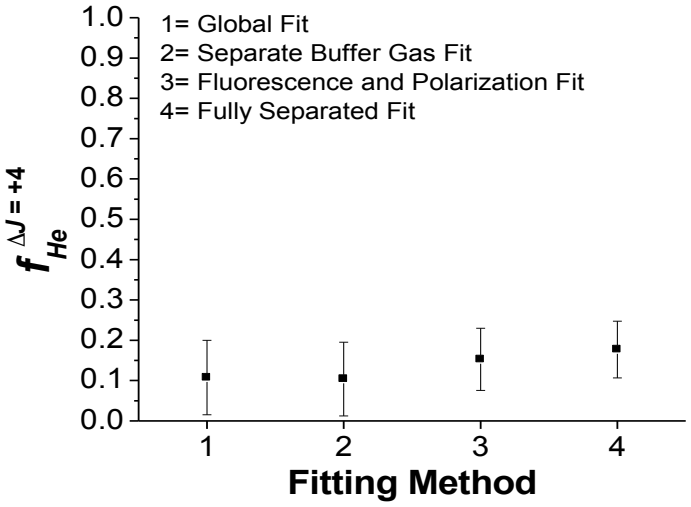

(d) $\Delta J = +4$

Supplementary Material Fig. 6a: Plots of the fitted fraction of orientation destroyed $f_{He}^{\Delta J}$ for helium collisions following excitation of NaK molecules to the $2(A)^1\Sigma^+(v=16, J=30)$ level, for each of the fitting methods described in the text ($+4 \geq \Delta J \geq +1$).

$f_{He}^{\Delta J}$ for NaK $2(A)^1\Sigma^+(v=16, J=30)$

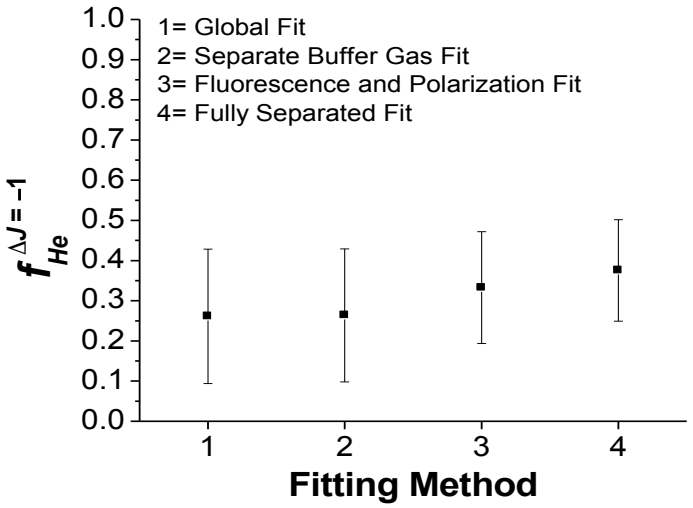

(a) $\Delta J = -1$

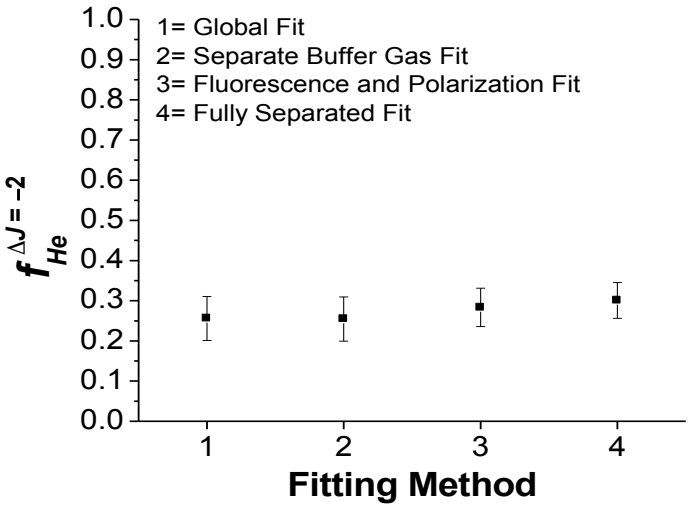

(b) $\Delta J = -2$

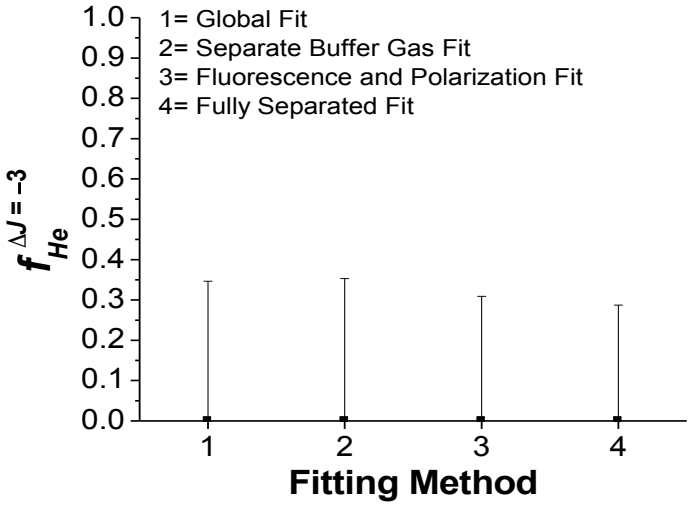

(c) $\Delta J = -3$

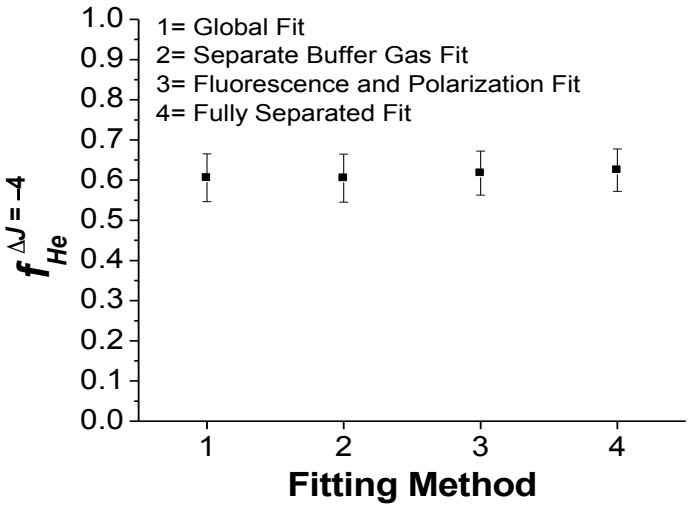

(d) $\Delta J = -4$

Supplementary Material Fig. 6b: Plots of the fitted fraction of orientation destroyed $f_{He}^{\Delta J}$ for helium collisions following excitation of NaK molecules to the $2(A)^1\Sigma^+(v=16, J=30)$ level, for each of the fitting methods described in the text ($-4 \le \Delta J \le -1$).

$f_K^{\Delta J}$ for NaK $2(A)^1\Sigma^+(v=16, J=30)$

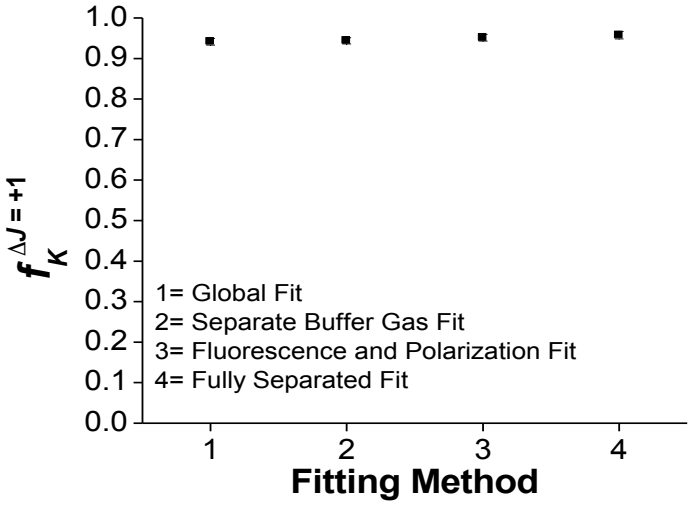

(a) $\Delta J = +1$

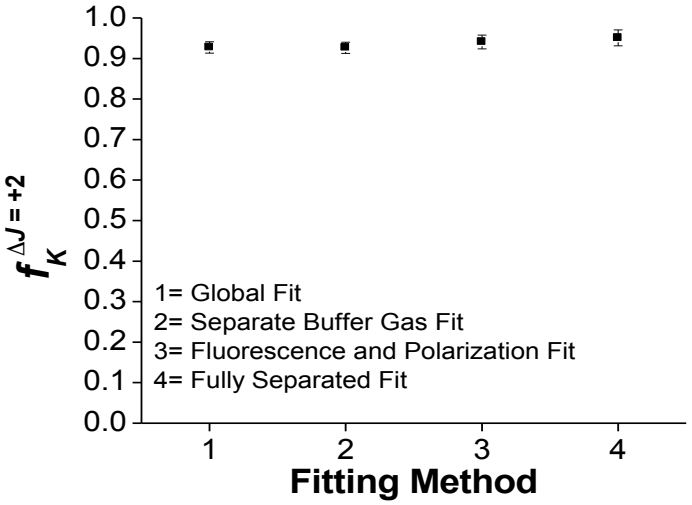

(b) $\Delta J = +2$

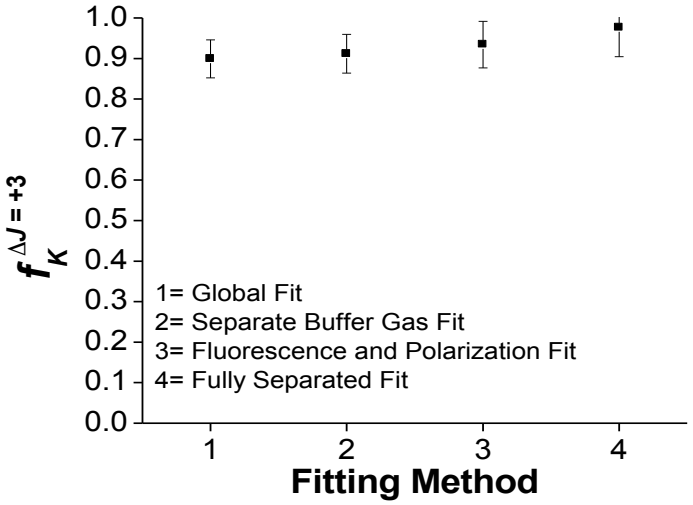

(c) $\Delta J = +3$

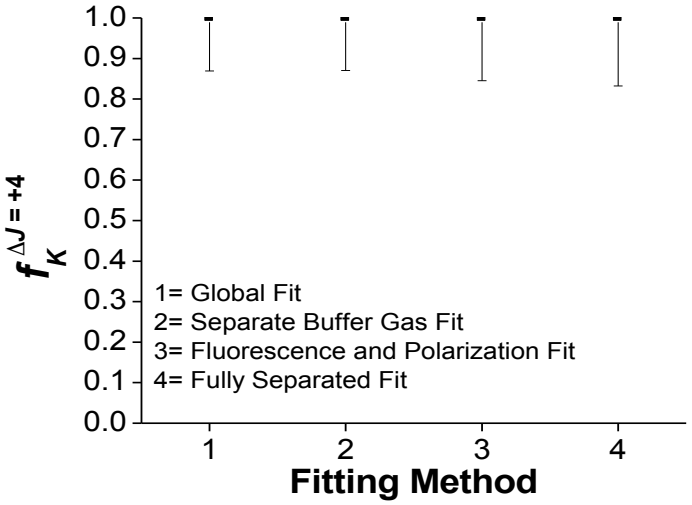

(d) $\Delta J = +4$

Supplementary Material Fig. 7a: Plots of the fitted fraction of orientation destroyed $f_K^{\Delta J}$ for potassium collisions following excitation of NaK molecules to the $2(A)^1\Sigma^+(v=16, J=30)$ level, for each of the fitting methods described in the text ($+4 \geq \Delta J \geq +1$).

$f_K^{\Delta J}$ for NaK $2(A)^1\Sigma^+(v=16, J=30)$

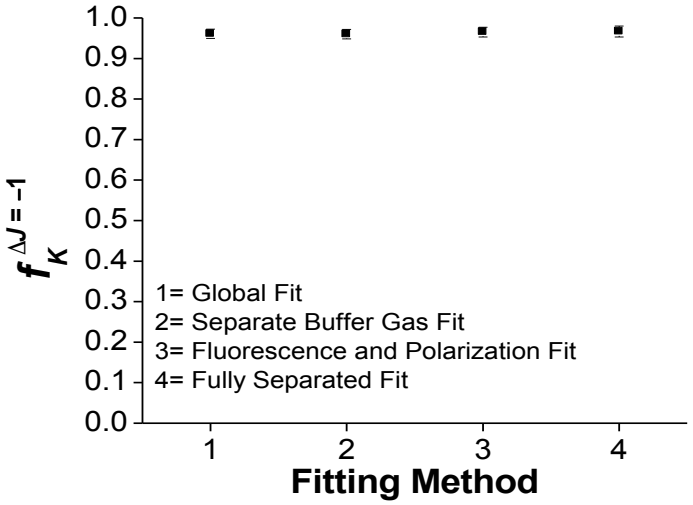

(a) $\Delta J = -1$

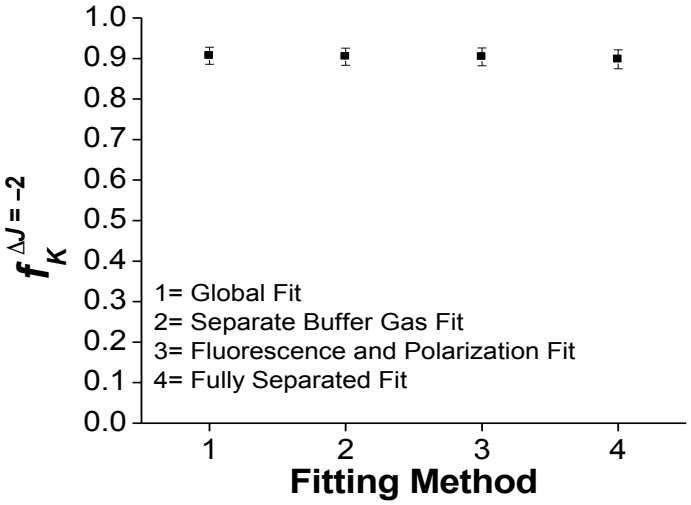

(b) $\Delta J = -2$

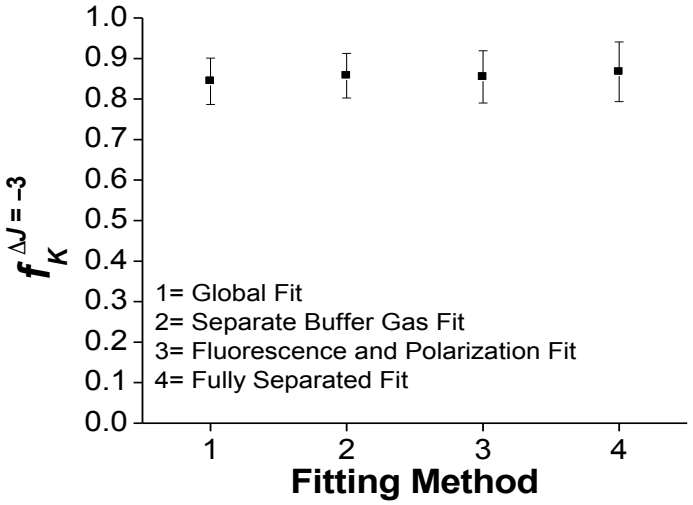

(c) $\Delta J = -3$

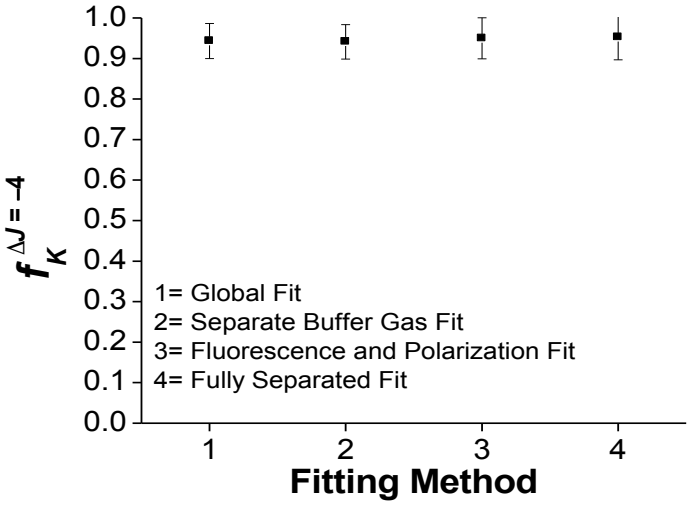

(d) $\Delta J = -4$

Supplementary Material Fig. 7b: Plots of the fitted fraction of orientation destroyed $f_K^{\Delta J}$ for potassium collisions following excitation of NaK molecules to the $2(A)^1\Sigma^+(v=16, J=30)$ level, for each of the fitting methods described in the text ($-4 \le \Delta J \le -1$).

g'_p for NaK $2(A)^1\Sigma^+(v=16, J=30)$

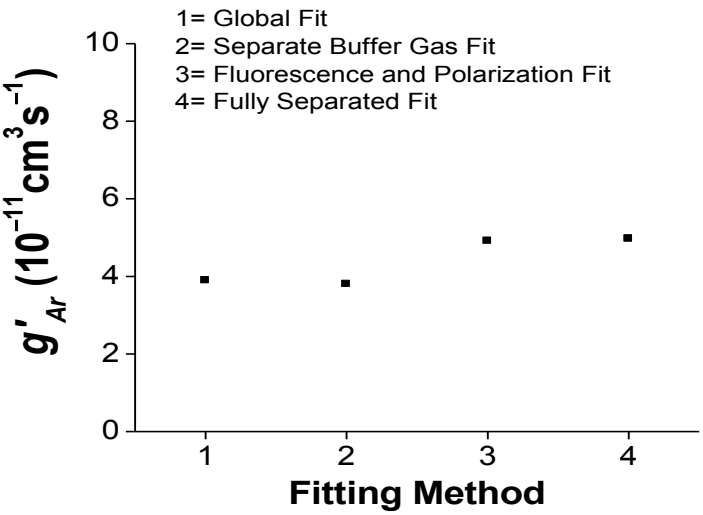

(a) g'_{Ar}

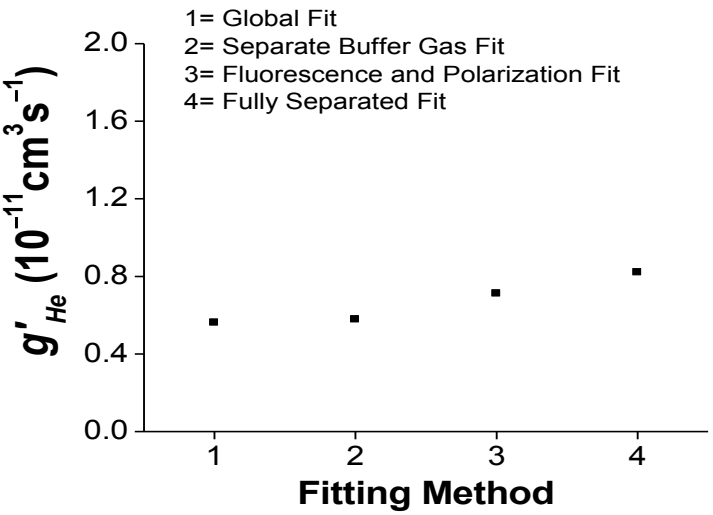

(b) g'_{He}

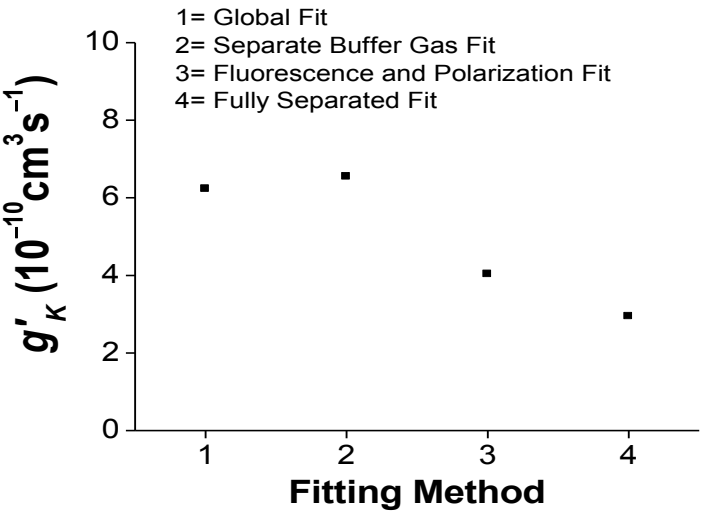

(c) g'_K

Supplementary Material Fig. 8: Plots of the fitted rate coefficients for total destruction of orientation g'_p following excitation of NaK molecules to the $2(A)^1\Sigma^+(v=16, J=30)$ level, for each of the fitting methods described in the text. a) argon, b) helium, and c) potassium collisions.

R_F vs. n_{He} for NaK $2(A)^1\Sigma^+(v=16, J=30)$, $\Delta J = +1$

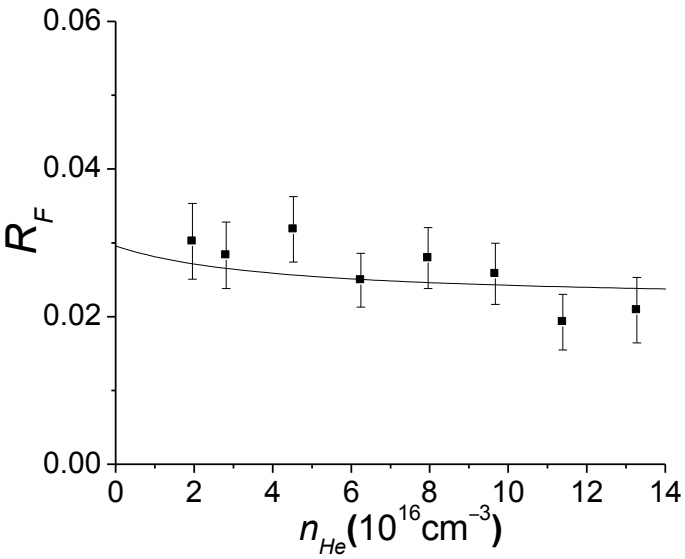

(a) $n_K = 2.75 \times 10^{15}$ cm^{-3}

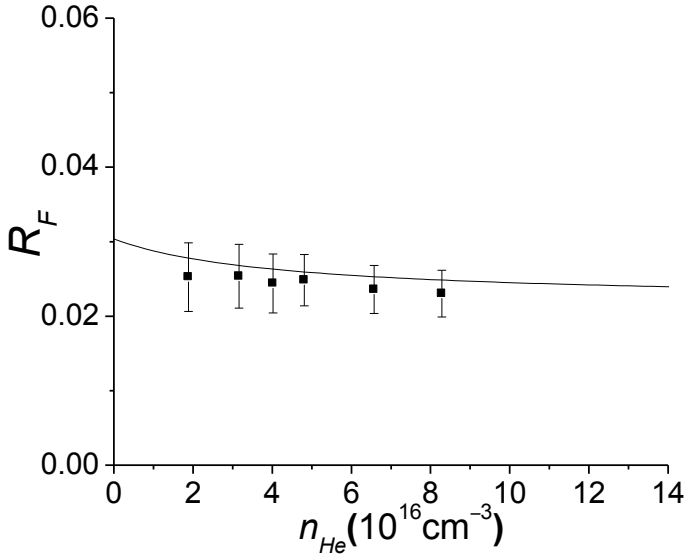

(b) $n_K = 2.88 \times 10^{15}$ cm^{-3}

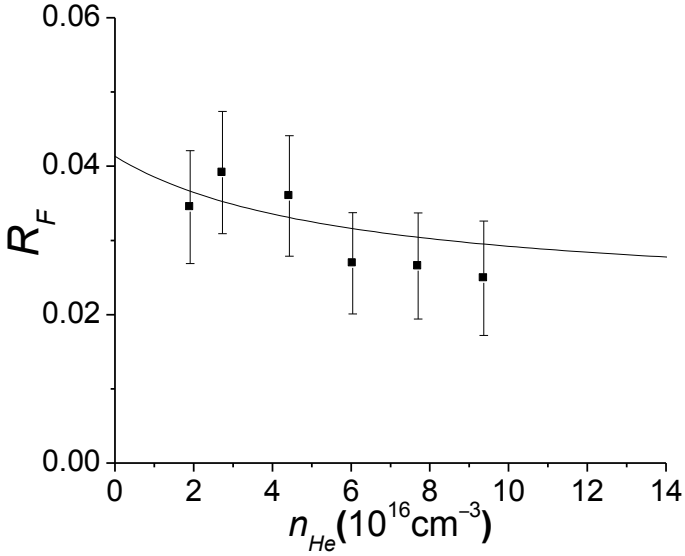

(c) $n_K = 5.44 \times 10^{15}$ cm^{-3}

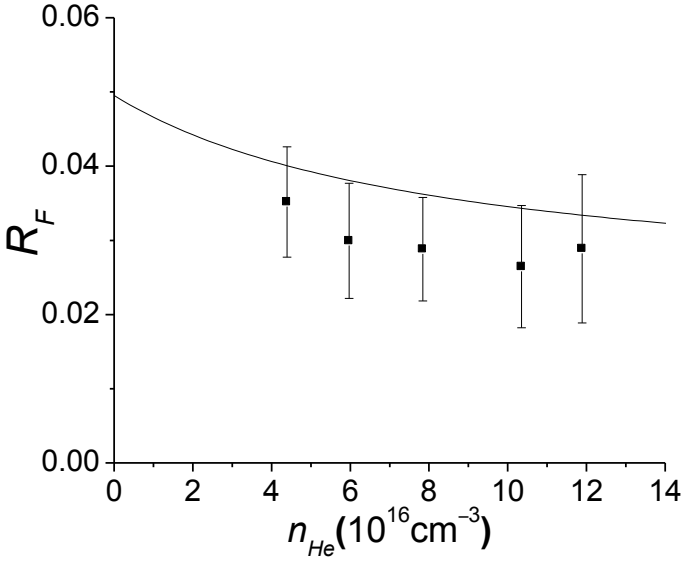

(d) $n_K = 9.20 \times 10^{15}$ cm^{-3}

Supplementary Material Fig. 9: Plots of fluorescence ratio data (R_F) versus helium density for $\Delta J = +1$ collisions of NaK $2(A)^1\Sigma^+(v=16, J=30)$ molecules with helium and potassium perturbers. Each panel represents a fixed potassium density n_K. In this, and subsequent plots, the calculated R_F values (solid curves) were obtained using the global fit parameters given in Table 1 of the paper (also listed in Supplementary Table 1).

R_F vs. n_{He} for NaK $2(A)^1\Sigma^+(v=16, J=30)$, $\Delta J = +2$

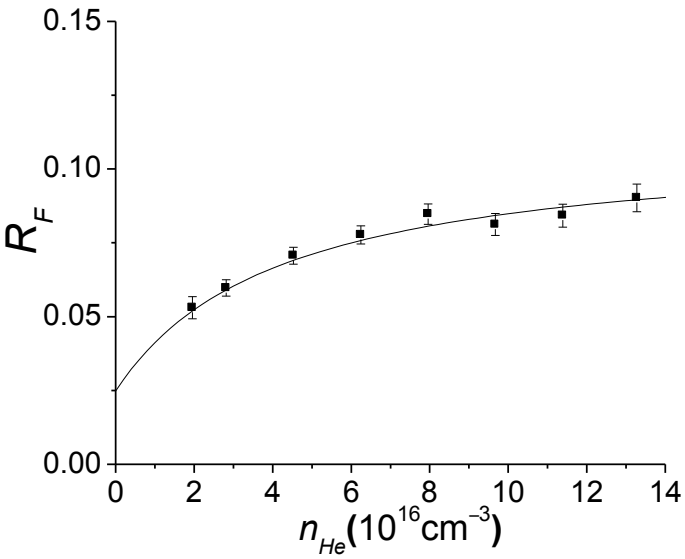

(a) $n_K = 2.75 \times 10^{15}$ cm^{-3}

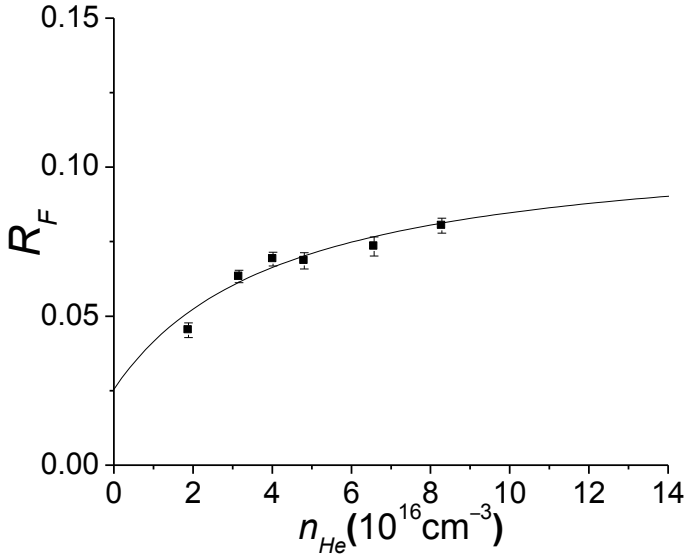

(b) $n_K = 2.88 \times 10^{15}$ cm^{-3}

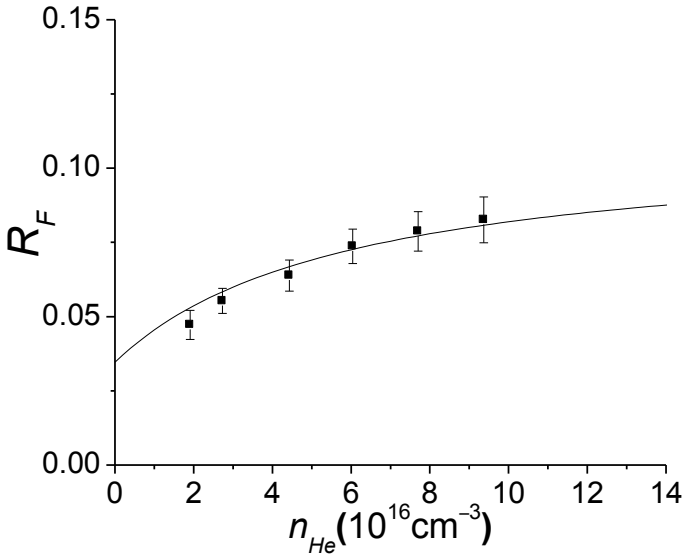

(c) $n_K = 5.44 \times 10^{15}$ cm^{-3}

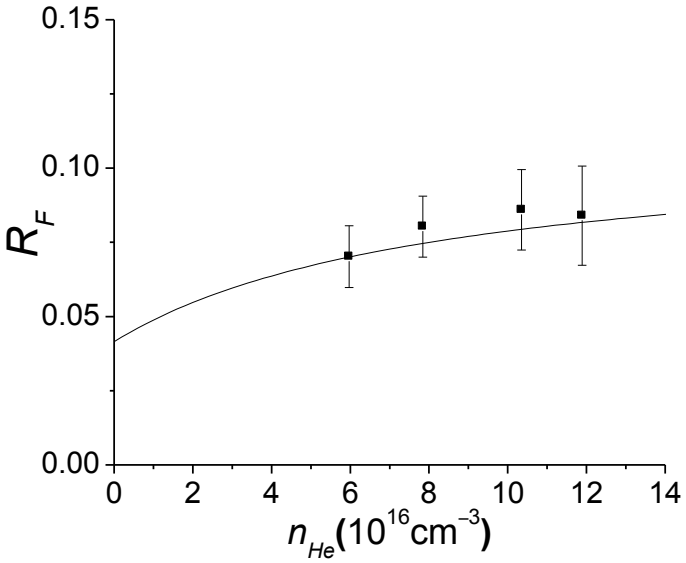

(d) $n_K = 9.20 \times 10^{15}$ cm^{-3}

Supplementary Material Fig. 10: Plots of fluorescence ratio data (R_F) versus helium density for ΔJ = +2 collisions of NaK $2(A)^1\Sigma^+(v=16, J=30)$ molecules with helium and potassium perturbers. Each panel represents a fixed potassium density n_K.

R_F vs. n_{He} for NaK $2(A)^1\Sigma^+(v=16, J=30)$, $\Delta J = +3$

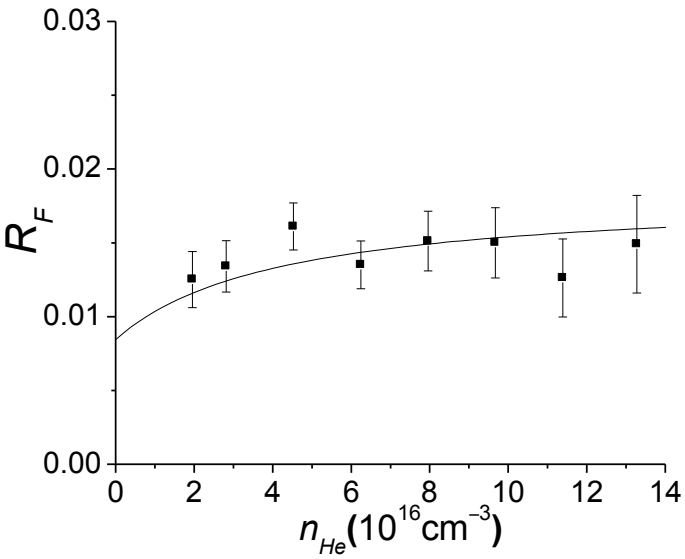

(a) $n_K = 2.75 \times 10^{15}$ cm^{-3}

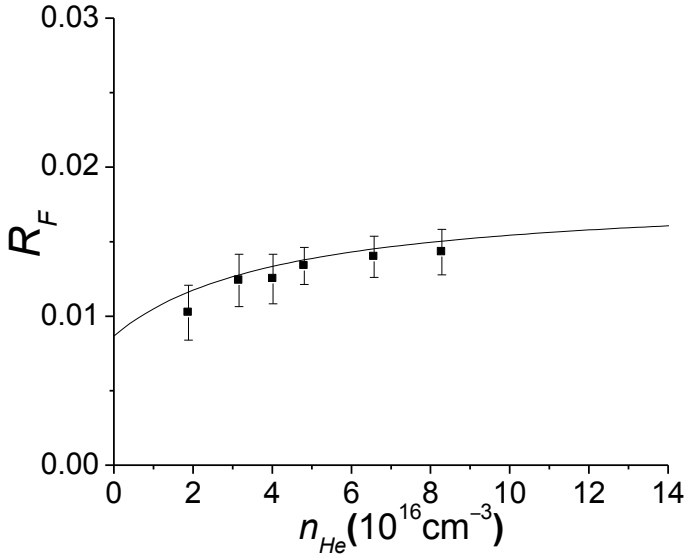

(b) $n_K = 2.88 \times 10^{15}$ cm^{-3}

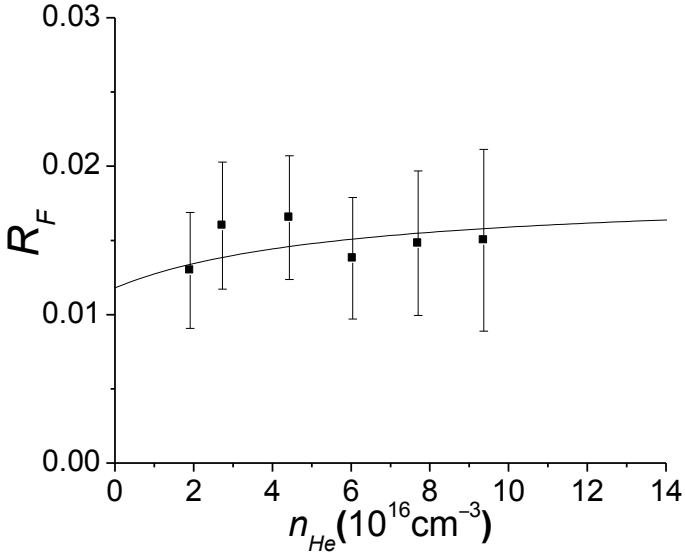

(c) $n_K = 5.44 \times 10^{15}$ cm^{-3}

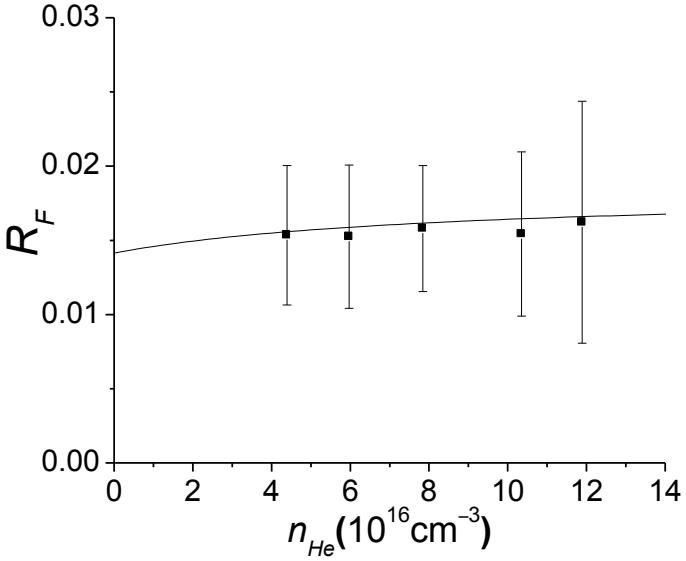

(d) $n_K = 9.20 \times 10^{15}$ cm^{-3}

Supplementary Material Fig. 11: Plots of fluorescence ratio data (R_F) versus helium density for ΔJ = +3 collisions of NaK $2(A)^1\Sigma^+(v=16, J=30)$ molecules with helium and potassium perturbers. Each panel represents a fixed potassium density n_K.

R_F vs. n_{He} for NaK $2(A)^1\Sigma^+(v=16, J=30)$, $\Delta J = +4$

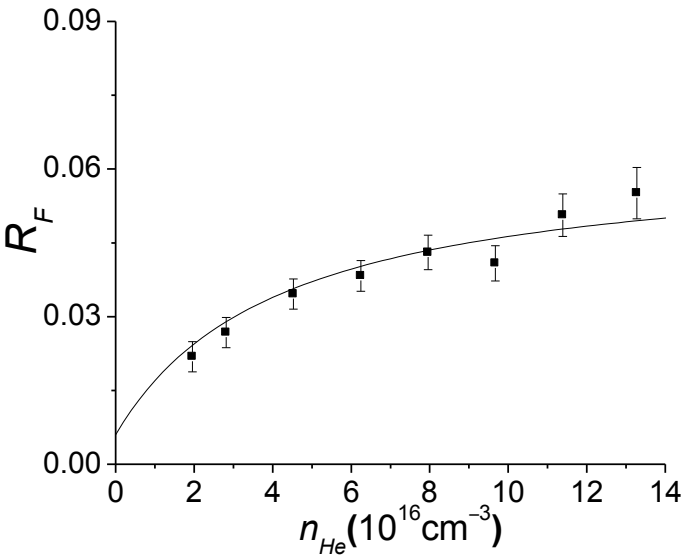

(a) $n_K = 2.75 \times 10^{15}$ cm^{-3}

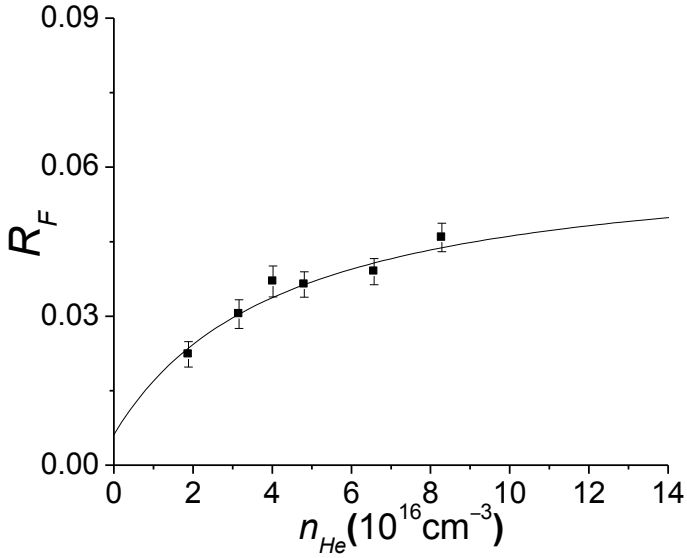

(b) $n_K = 2.88 \times 10^{15}$ cm^{-3}

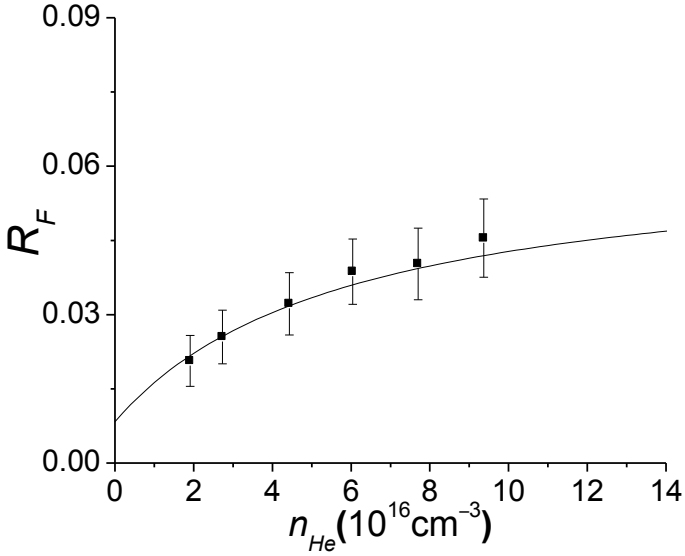

(c) $n_K = 5.44 \times 10^{15}$ cm^{-3}

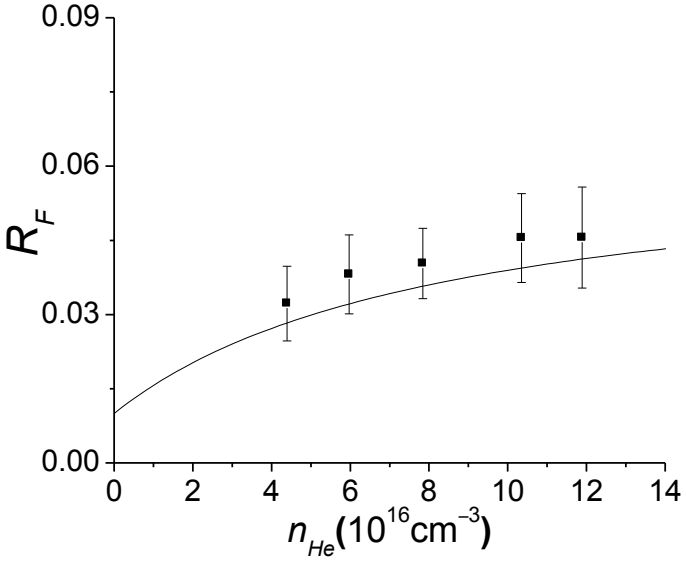

(d) $n_K = 9.20 \times 10^{15}$ cm^{-3}

Supplementary Material Fig. 12: Plots of fluorescence ratio data (R_F) versus helium density for ΔJ = +4 collisions of NaK $2(A)^1\Sigma^+(v=16, J=30)$ molecules with helium and potassium perturbers. Each panel represents a fixed potassium density n_K.

R_F vs. n_{He} for NaK $2(A)^1\Sigma^+(v=16, J=30)$, $\Delta J = -1$

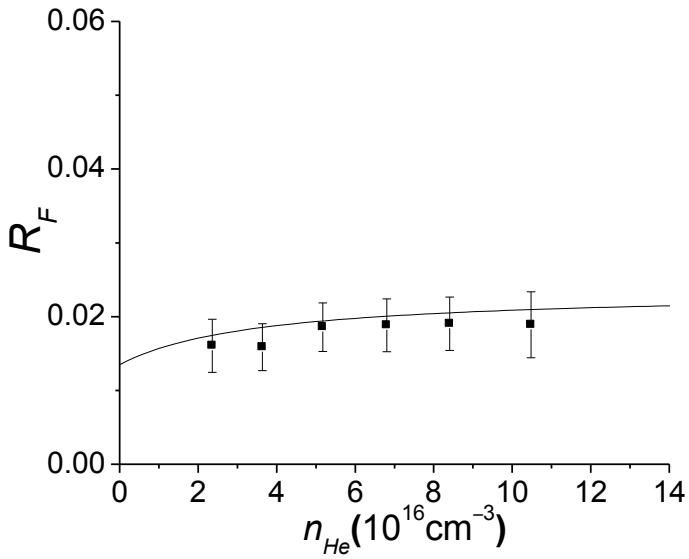

(a) $n_K = 1.80 \times 10^{15}$ cm^{-3}

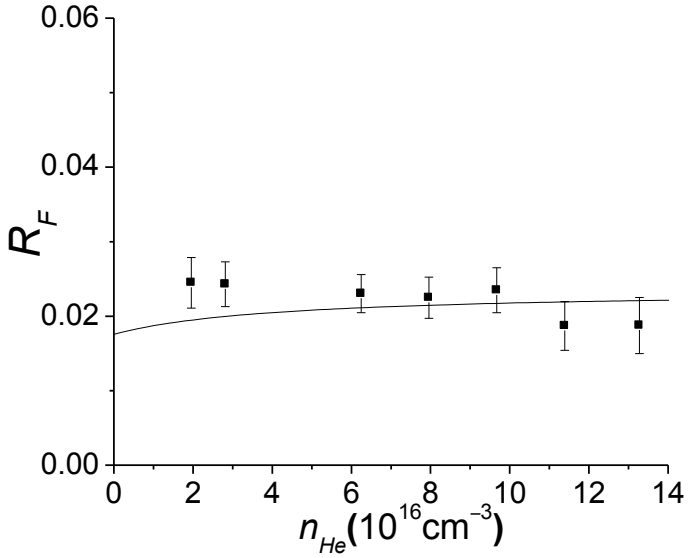

(b) $n_K = 2.75 \times 10^{15}$ cm^{-3}

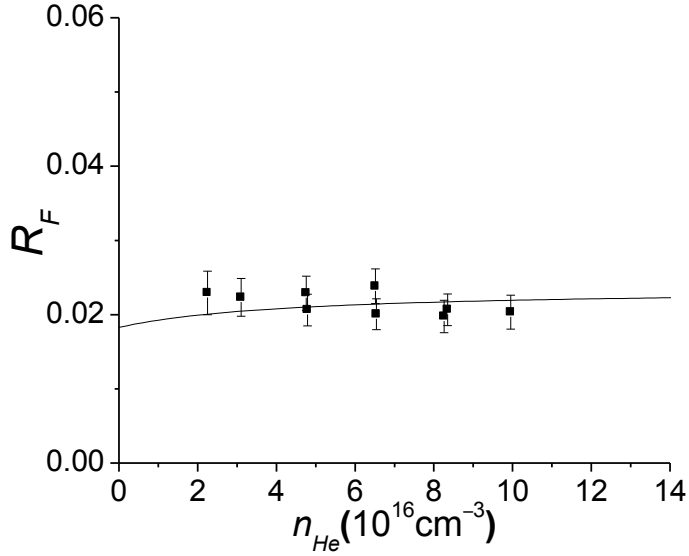

(c) $n_K = 2.94 \times 10^{15}$ cm^{-3}

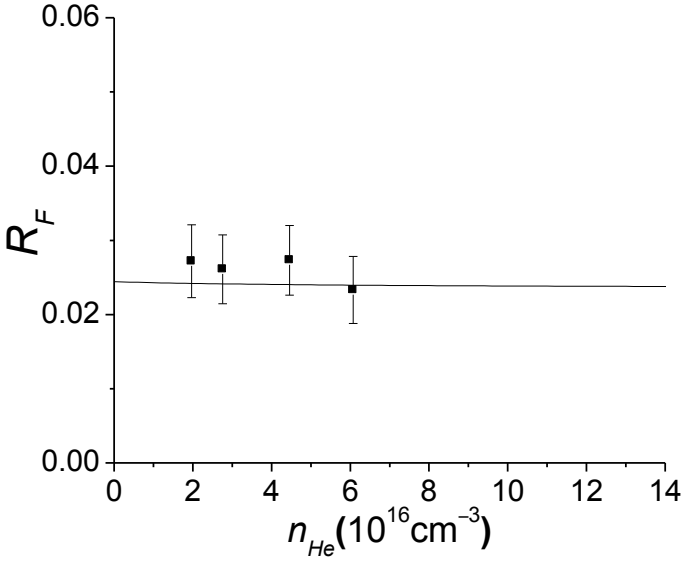

(d) $n_K = 5.37 \times 10^{15}$ cm^{-3}

Supplementary Material Fig. 13: Plots of fluorescence ratio data (R_F) versus helium density for $\Delta J = -1$ collisions of NaK $2(A)^1\Sigma^+(v=16, J=30)$ molecules with helium and potassium perturbers. Each panel represents a fixed potassium density n_K.

R_F vs. n_{He} for NaK $2(A)^1\Sigma^+(v=16, J=30)$, $\Delta J = -2$

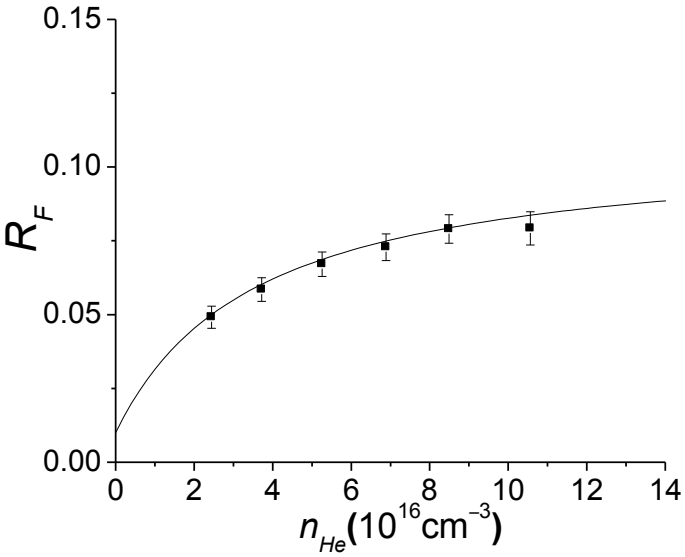

(a) $n_K = 1.80 \times 10^{15}$ cm^{-3}

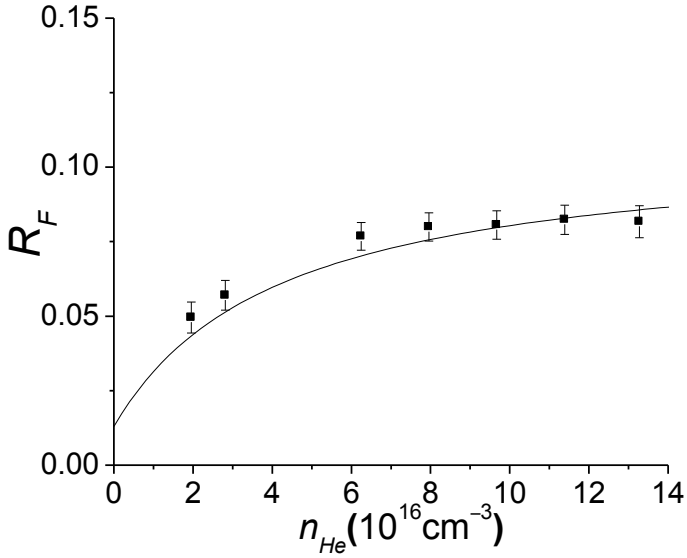

(b) $n_K = 2.75 \times 10^{15}$ cm^{-3}

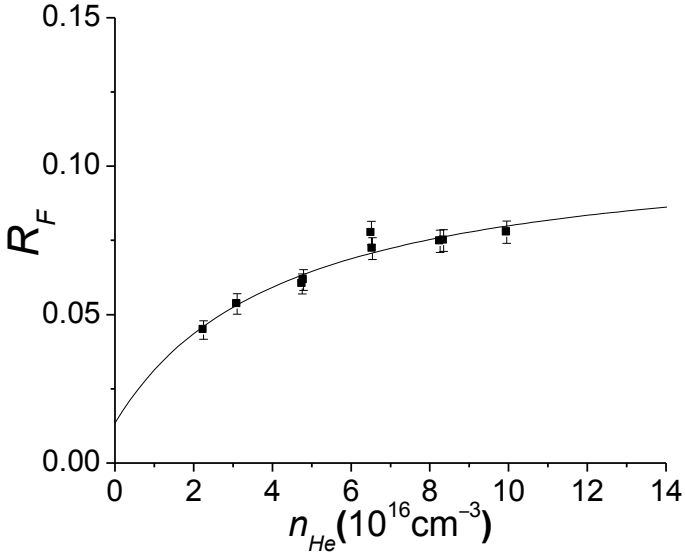

(c) $n_K = 2.94 \times 10^{15}$ cm^{-3}

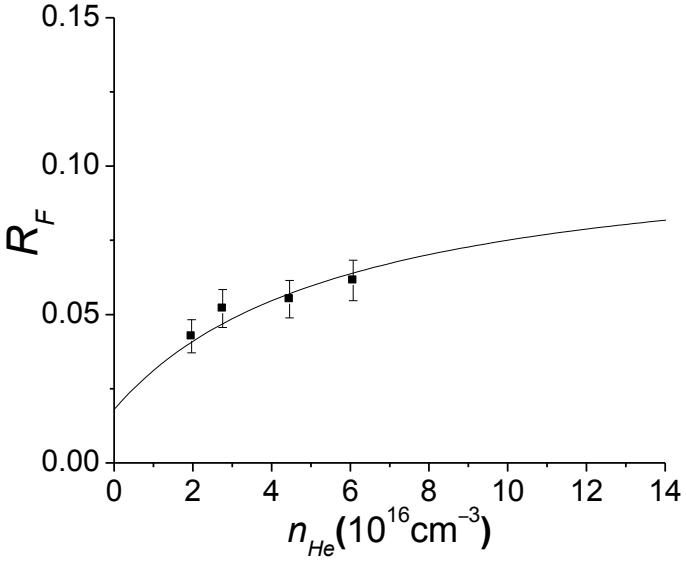

(d) $n_K = 5.37 \times 10^{15}$ cm^{-3}

Supplementary Material Fig. 14: Plots of fluorescence ratio data (R_F) versus helium density for $\Delta J = -2$ collisions of NaK $2(A)^1\Sigma^+(v=16, J=30)$ molecules with helium and potassium perturbers. Each panel represents a fixed potassium density n_K.

R_F vs. n_{He} for NaK $2(A)^1\Sigma^+(v=16, J=30)$, $\Delta J = -3$

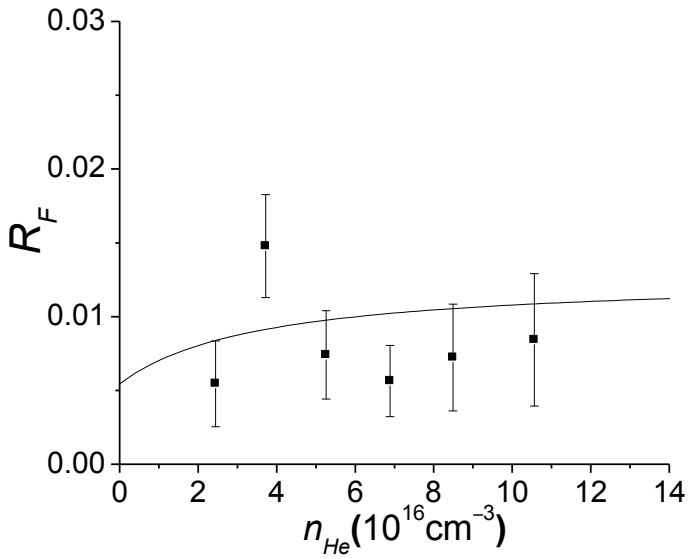

(a) $n_K = 1.80 \times 10^{15}$ cm^{-3}

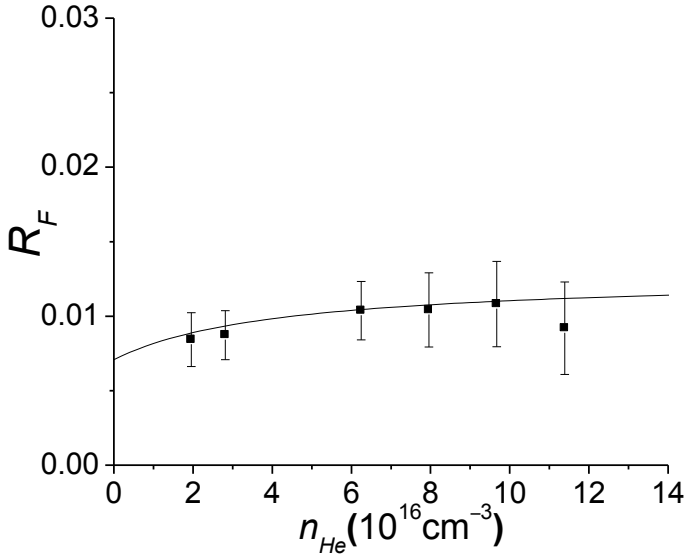

(b) $n_K = 2.75 \times 10^{15}$ cm^{-3}

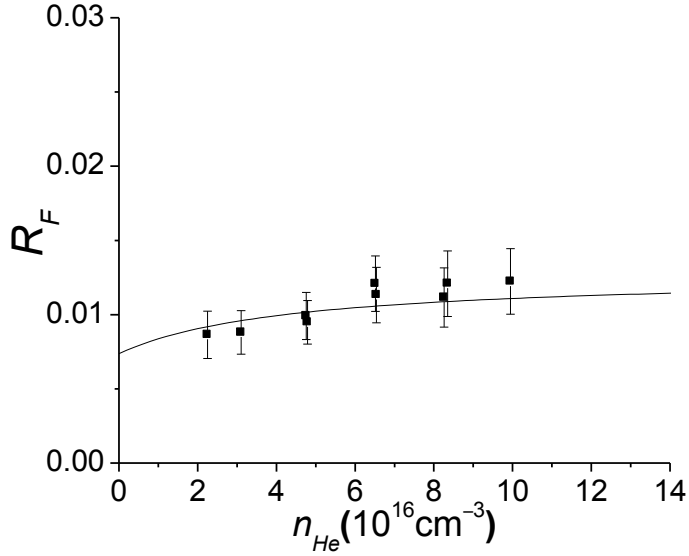

(c) $n_K = 2.94 \times 10^{15}$ cm^{-3}

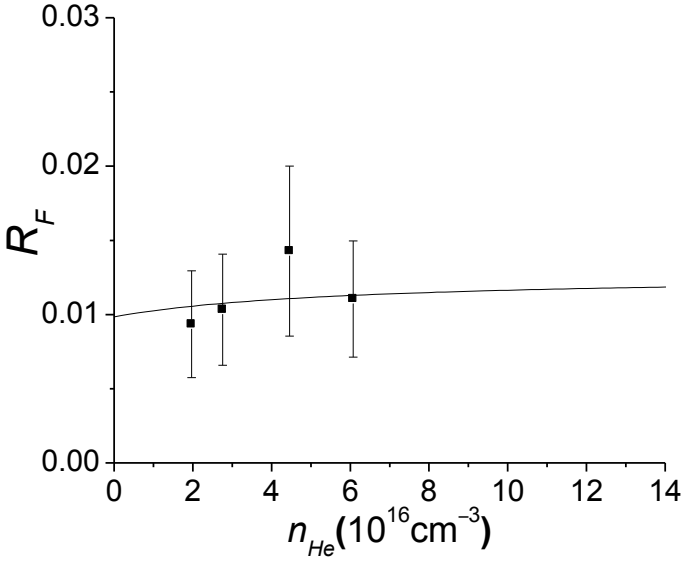

(d) $n_K = 5.37 \times 10^{15}$ cm^{-3}

Supplementary Material Fig. 15: Plots of fluorescence ratio data (R_F) versus helium density for $\Delta J = -3$ collisions of NaK $2(A)^1\Sigma^+(v=16, J=30)$ molecules with helium and potassium perturbers. Each panel represents a fixed potassium density n_K.

R_F vs. n_{He} for NaK $2(A)^1\Sigma^+(v=16, J=30)$, $\Delta J = -4$

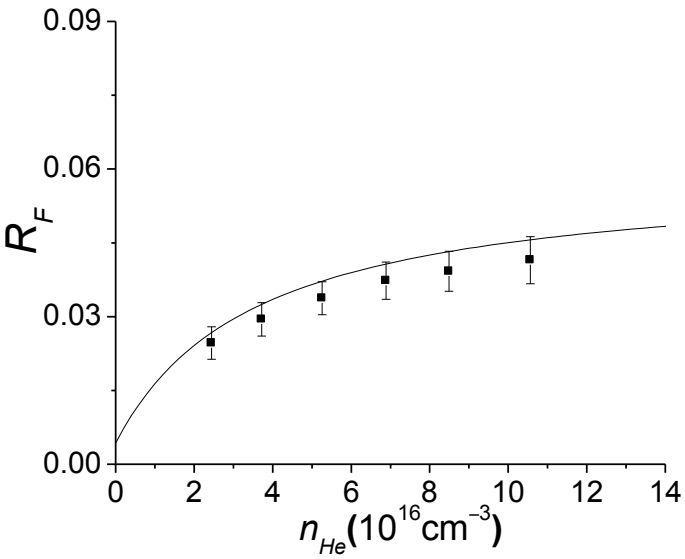

(a) $n_K = 1.80 \times 10^{15}$ cm^{-3}

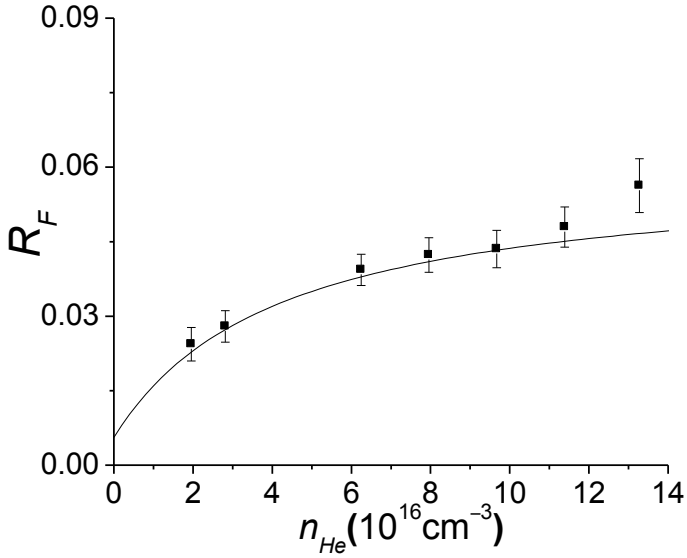

(b) $n_K = 2.75 \times 10^{15}$ cm^{-3}

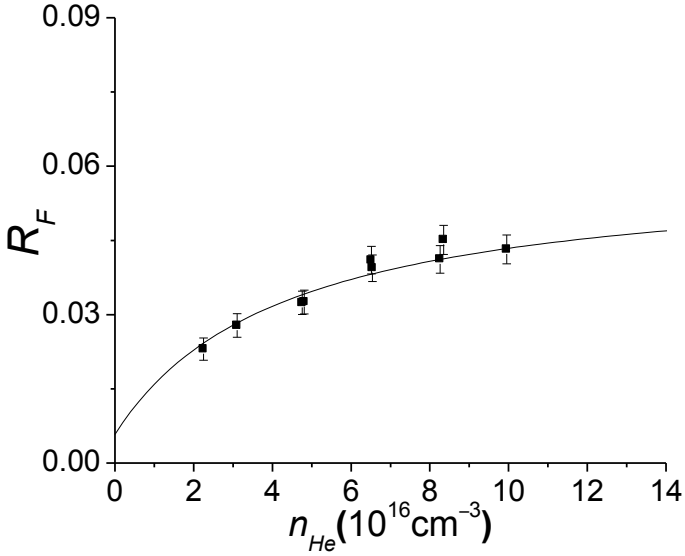

(c) $n_K = 2.94 \times 10^{15}$ cm^{-3}

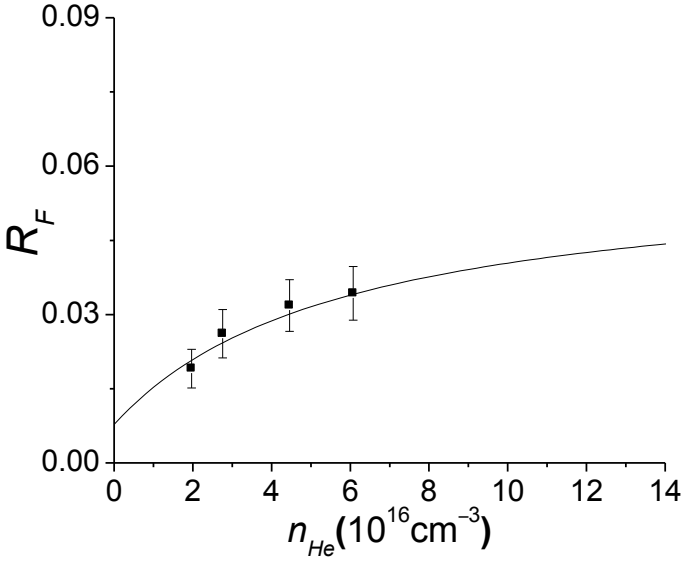

(d) $n_K = 5.37 \times 10^{15}$ cm^{-3}

Supplementary Material Fig. 16: Plots of fluorescence ratio data (R_F) versus helium density for $\Delta J = -4$ collisions of NaK $2(A)^1\Sigma^+(v=16, J=30)$ molecules with helium and potassium perturbers. Each panel represents a fixed potassium density n_K.

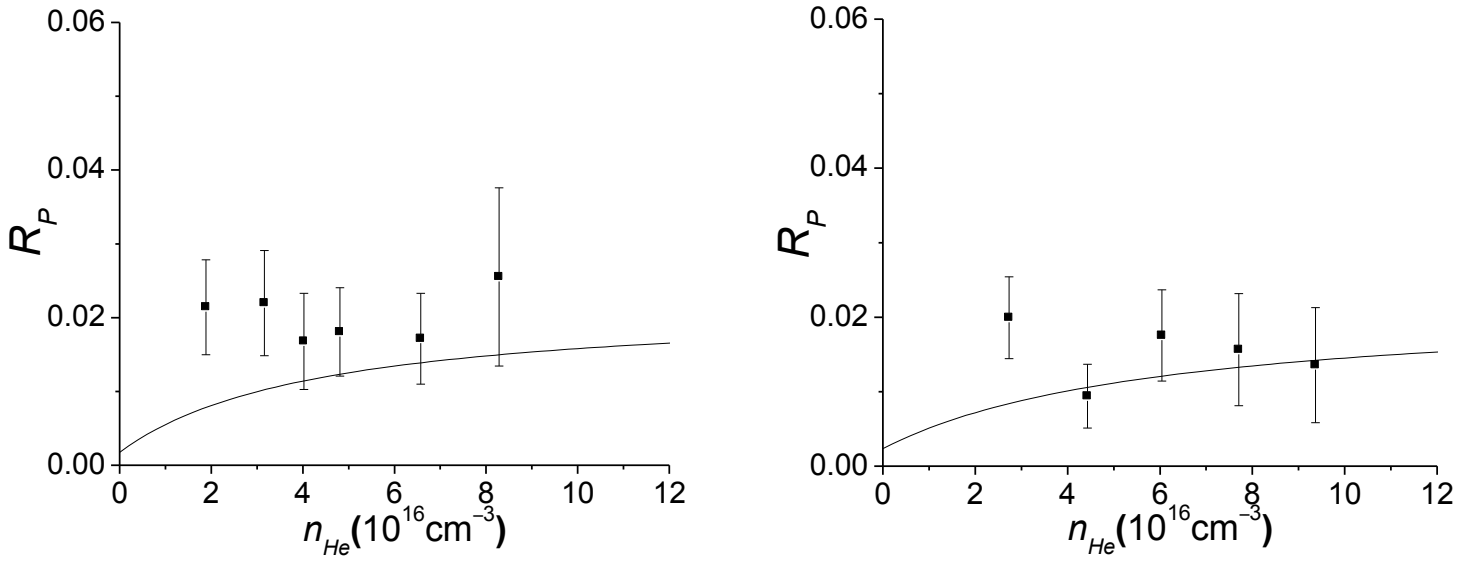

(a) $n_K = 2.88 \times 10^{15}$ cm^{-3} (b) $n_K = 5.44 \times 10^{15}$ cm^{-3}

Supplementary Material Fig. 17: Plots of polarization spectroscopy ratio data (R_P) versus helium density for ΔJ = +1 collisions of NaK $2(A)^1\Sigma^+(v=16, J=30)$ molecules with helium and potassium perturbers. Each panel represents a fixed potassium density n_K. In this, and subsequent plots, the calculated R_P values (solid curves) were obtained using the global fit parameters given in Tables 1 and 2 of the paper (also listed in Supplementary Tables 1 and 2).

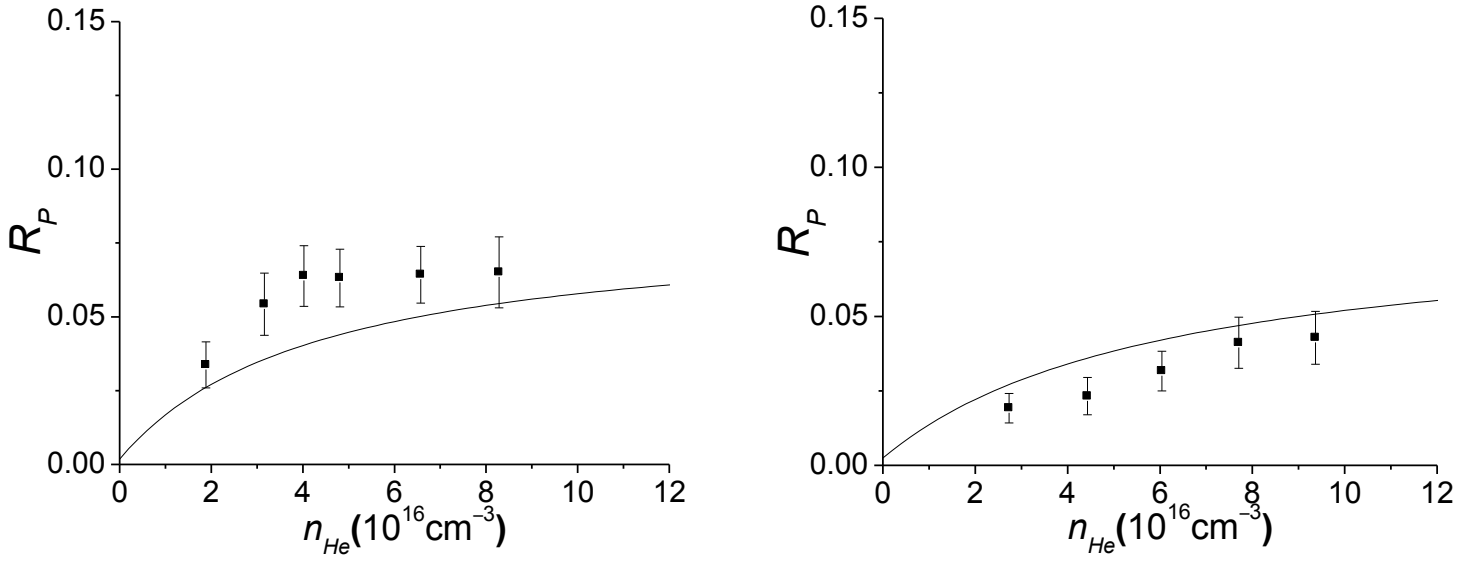

(a) $n_K = 2.88 \times 10^{15}$ cm^{-3} (b) $n_K = 5.44 \times 10^{15}$ cm^{-3}

Supplementary Material Fig. 18: Plots of polarization spectroscopy ratio data (R_P) versus helium density for ΔJ = +2 collisions of NaK $2(A)^1\Sigma^+(v=16, J=30)$ molecules with helium and potassium perturbers. Each panel represents a fixed potassium density n_K.

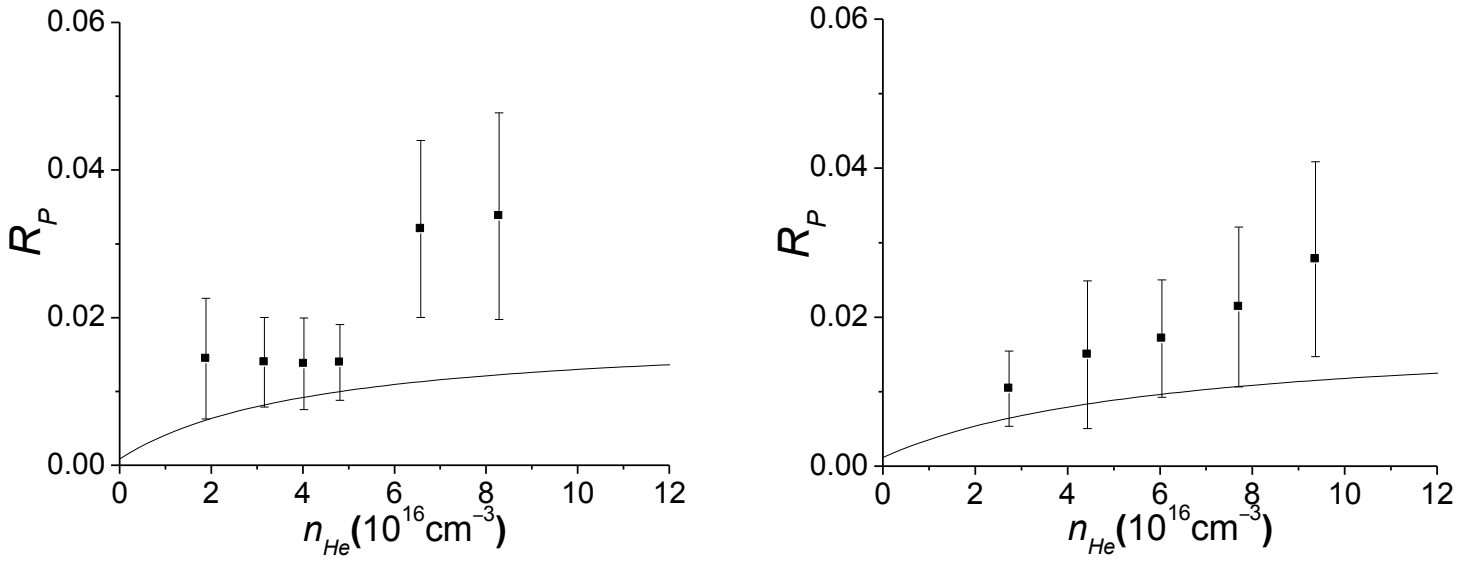

(a) $n_K = 2.88 \times 10^{15}$ cm^{-3} (b) $n_K = 5.44 \times 10^{15}$ cm^{-3}

Supplementary Material Fig. 19: Plots of polarization spectroscopy ratio data (R_P) versus helium density for ΔJ = +3 collisions of NaK 2$(A)^1\Sigma^+(v$=16, J=30) molecules with helium and potassium perturbers. Each panel represents a fixed potassium density n_K.

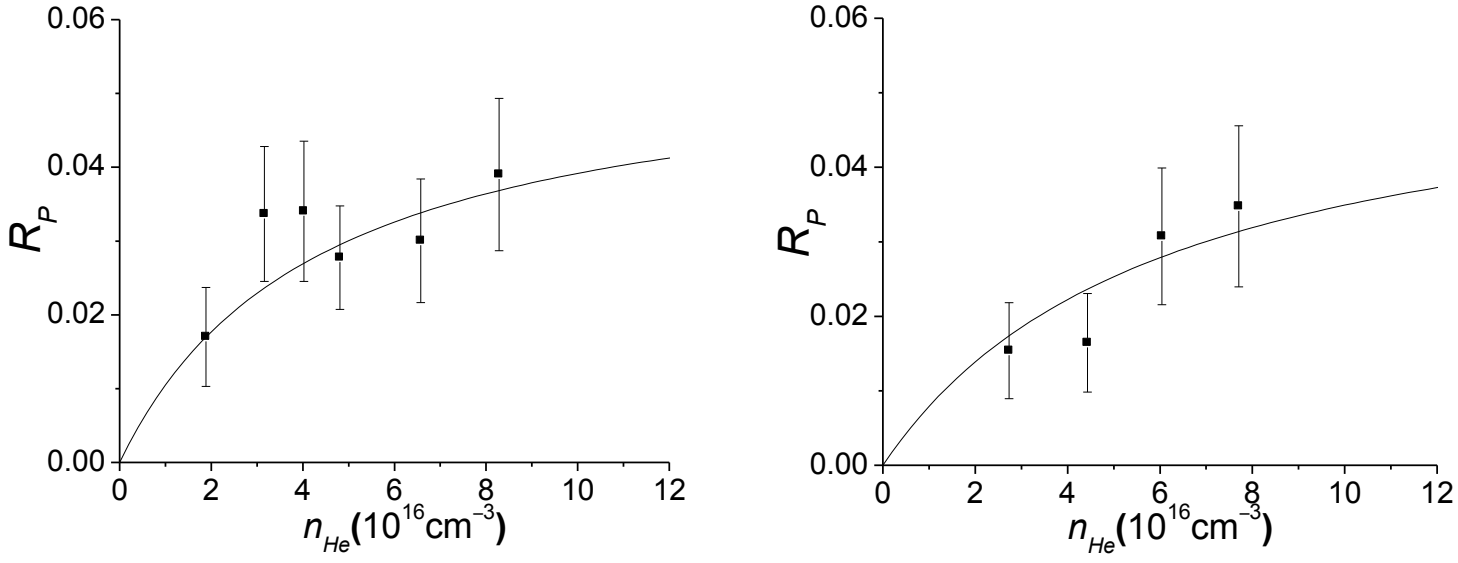

(a) $n_K = 2.88 \times 10^{15}$ cm^{-3} (b) $n_K = 5.44 \times 10^{15}$ cm^{-3}

Supplementary Material Fig. 20: Plots of polarization spectroscopy ratio data (R_P) versus helium density for ΔJ = +4 collisions of NaK 2$(A)^1\Sigma^+(v$=16, J=30) molecules with helium and potassium perturbers. Each panel represents a fixed potassium density n_K.

R_P vs. n_{He} for NaK $2(A)^1\Sigma^+(v=16, J=30)$, $\Delta J = -1$

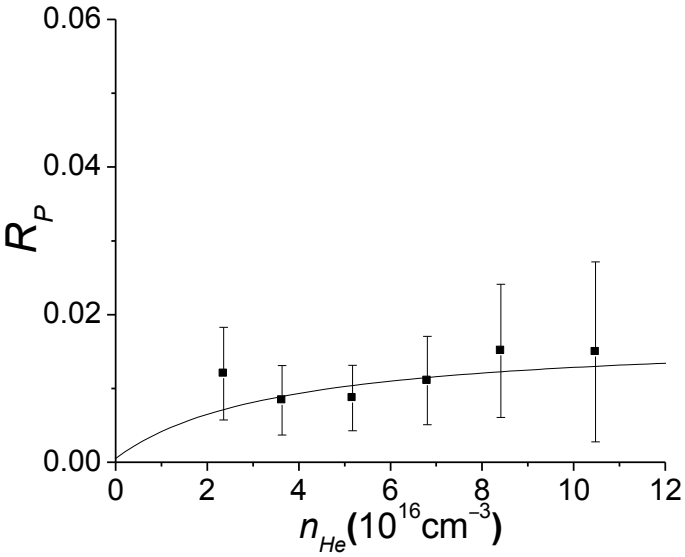

(a) $n_K = 1.80 \times 10^{15}$ cm^{-3}

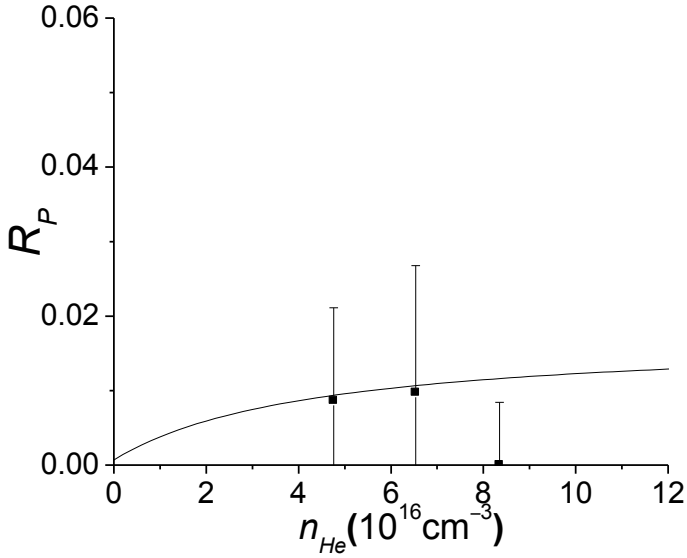

(b) $n_K = 2.88 \times 10^{15}$ cm^{-3}

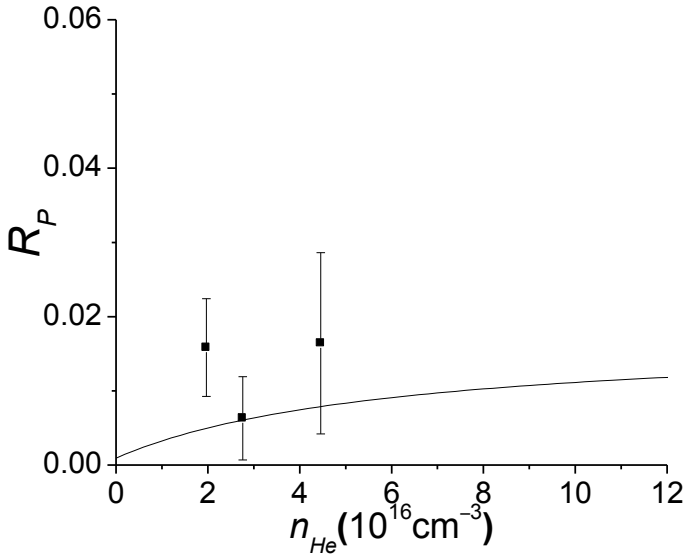

(c) $n_K = 5.37 \times 10^{15}$ cm^{-3}

Supplementary Material Fig. 21: Plots of polarization spectroscopy ratio data (R_P) versus helium density for $\Delta J = -1$ collisions of NaK $2(A)^1\Sigma^+(v=16, J=30)$ molecules with helium and potassium perturbers. Each panel represents a fixed potassium density n_K.

R_P vs. n_{He} for NaK $2(A)^1\Sigma^+(v=16, J=30)$, $\Delta J = -2$

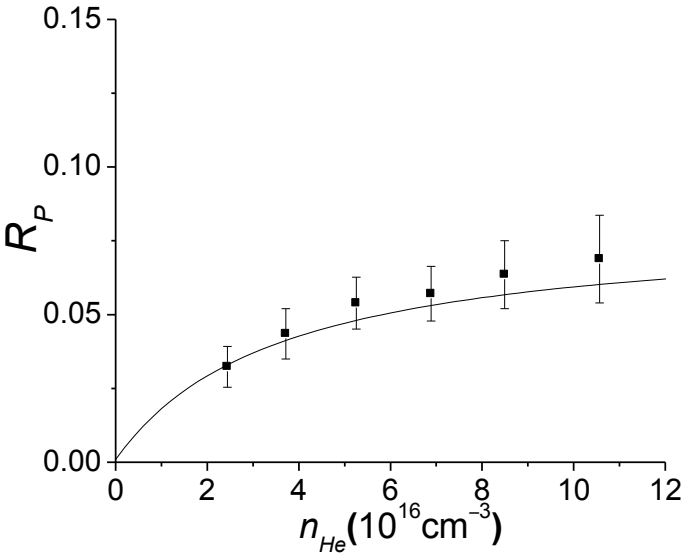

(a) $n_K = 1.80 \times 10^{15}$ cm^{-3}

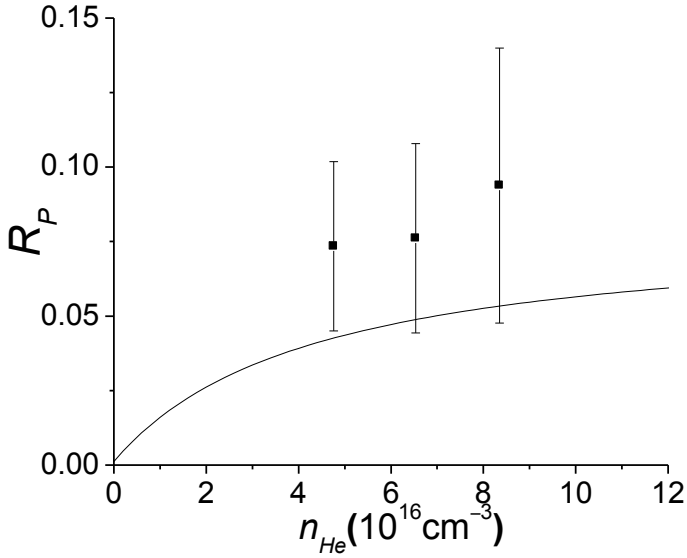

(b) $n_K = 2.88 \times 10^{15}$ cm^{-3}

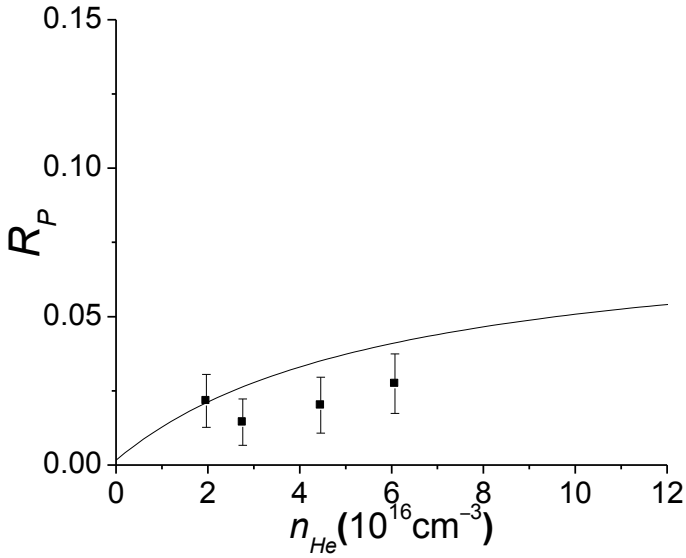

(c) $n_K = 5.37 \times 10^{15}$ cm^{-3}

Supplementary Material Fig. 22: Plots of polarization spectroscopy ratio data (R_P) versus helium density for $\Delta J = -2$ collisions of NaK $2(A)^1\Sigma^+(v=16, J=30)$ molecules with helium and potassium perturbers. Each panel represents a fixed potassium density n_K.

R_P vs. n_{He} for NaK $2(A)^1\Sigma^+(v=16, J=30)$, $\Delta J = -3$

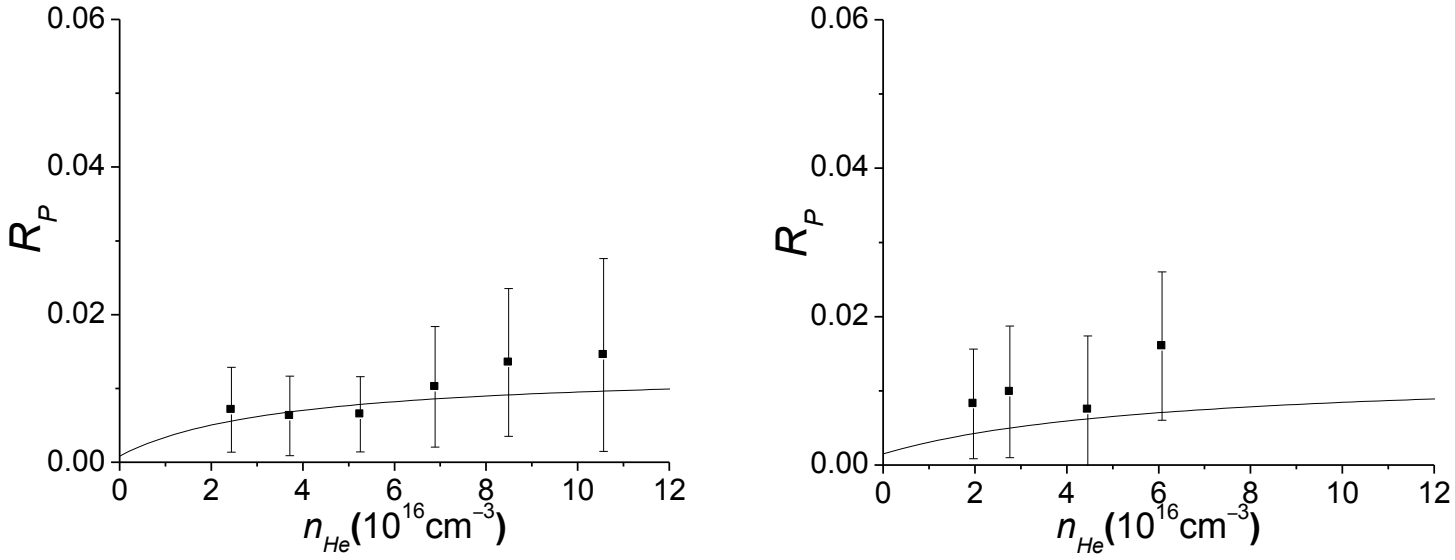

(a) $n_K = 1.80 \times 10^{15}$ cm^{-3} (b) $n_K = 5.37 \times 10^{15}$ cm^{-3}

Supplementary Material Fig. 23: Plots of polarization spectroscopy ratio data (R_P) versus helium density for $\Delta J = -3$ collisions of NaK $2(A)^1\Sigma^+(v=16, J=30)$ molecules with helium and potassium perturbers. Each panel represents a fixed potassium density n_K.

R_P vs. n_{He} for NaK $2(A)^1\Sigma^+(v=16, J=30)$, $\Delta J = -4$

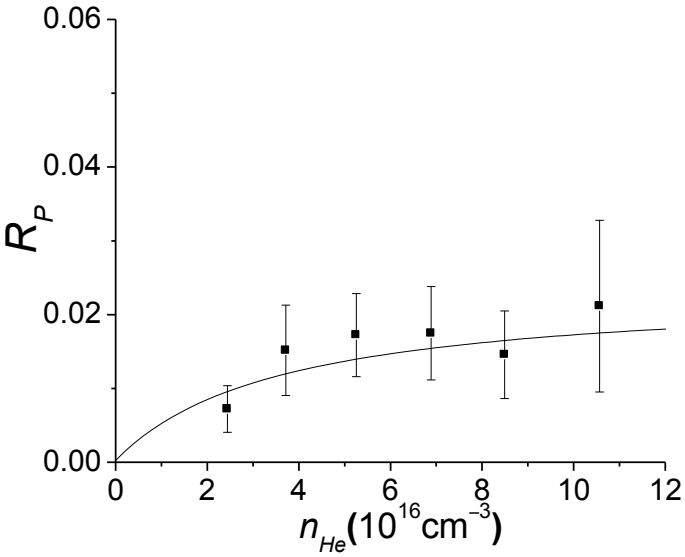

(a) $n_K = 1.80 \times 10^{15}$ cm^{-3}

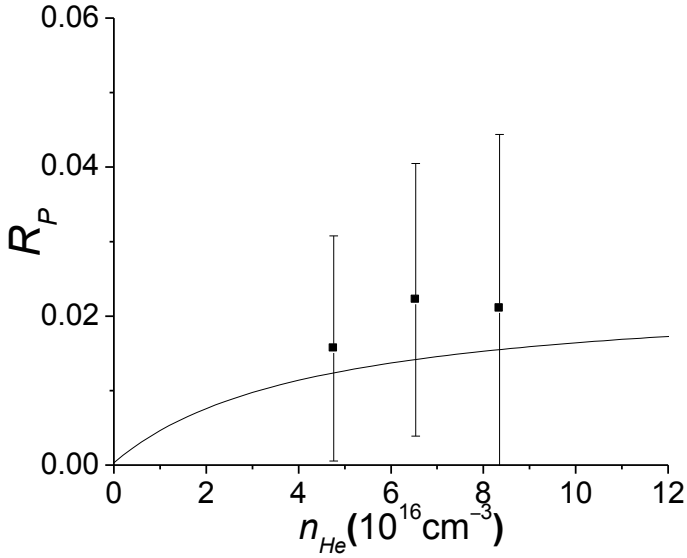

(b) $n_K = 2.88 \times 10^{15}$ cm^{-3}

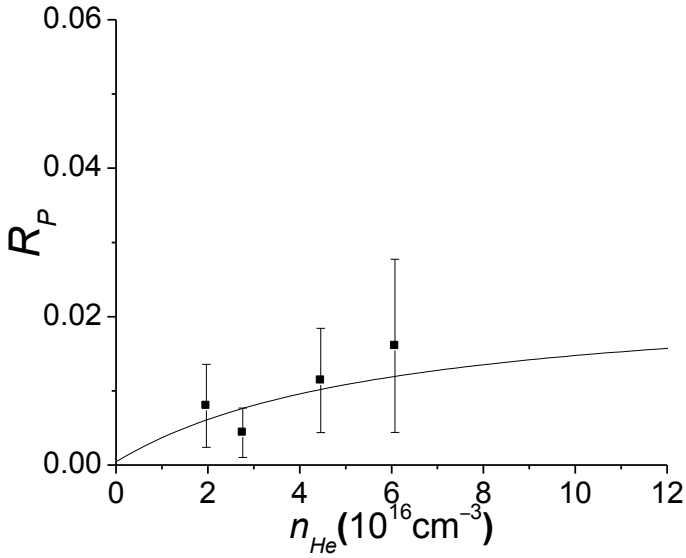

(c) $n_K = 5.37 \times 10^{15}$ cm^{-3}

Supplementary Material Fig. 24: Plots of polarization spectroscopy ratio data (R_P) versus helium density for $\Delta J = -4$ collisions of NaK $2(A)^1\Sigma^+(v=16, J=30)$ molecules with helium and potassium perturbers. Each panel represents a fixed potassium density n_K.

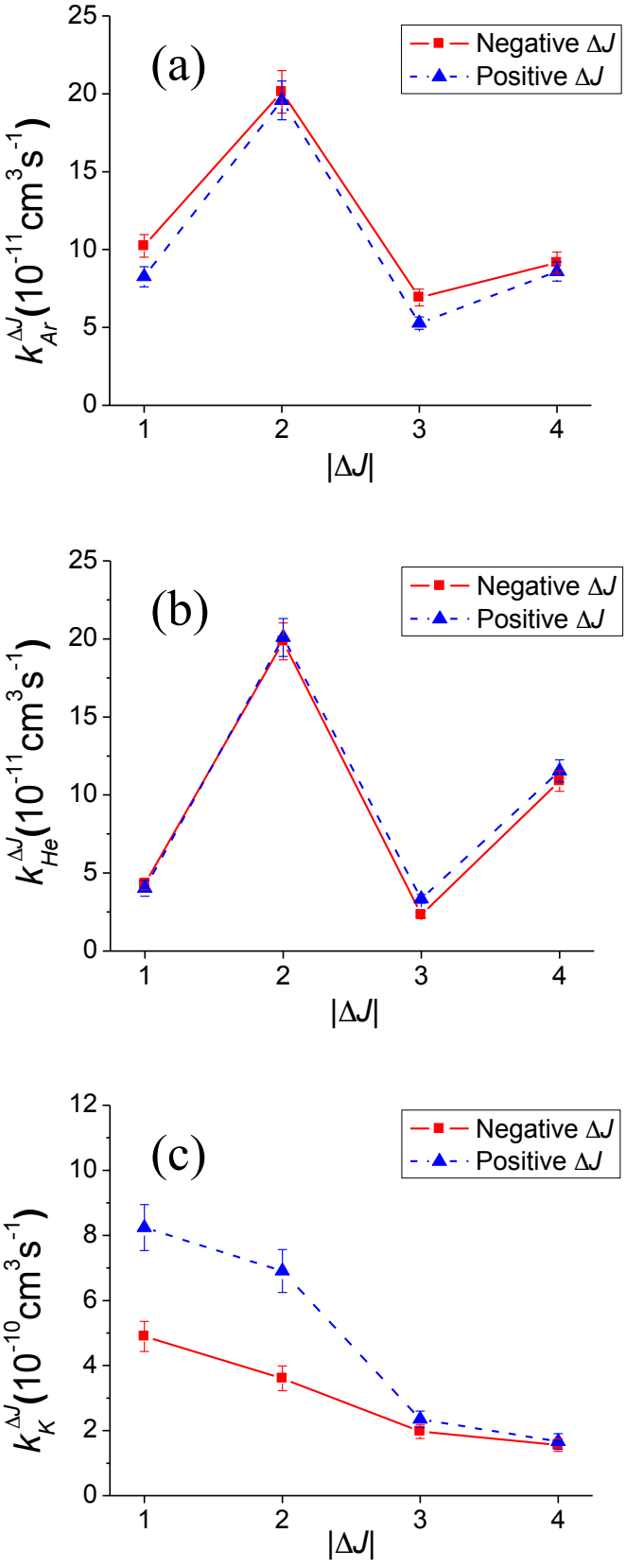

Supplementary Material Fig. 25: Experimental rate coefficients, $k_{Ar}^{\Delta J}$, $k_{He}^{\Delta J}$, and $k_{K}^{\Delta J}$, for collisions of NaK $2(A)^1\Sigma^+(v=16, J=30)$ molecules with (a) argon, (b) helium, and (c) potassium atoms as functions of ΔJ.

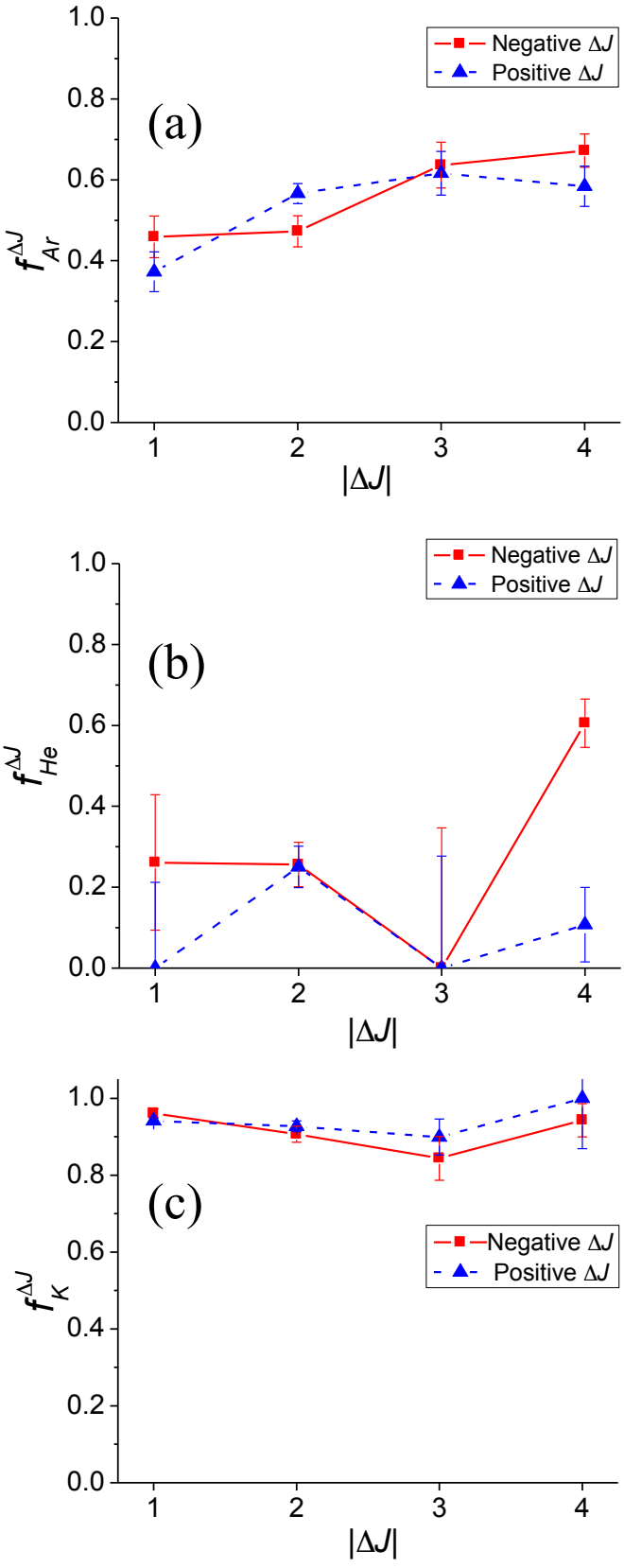

Supplementary Material Fig. 26: Experimental values for the fraction of orientation destroyed, $f_{Ar}^{\Delta J}$, $f_{He}^{\Delta J}$, and $f_{K}^{\Delta J}$, in rotationally inelastic collisions of NaK $2(A)^1\Sigma^+(v=16, J=30)$ molecules with (a) argon, (b) helium, and (c) potassium atoms as functions of ΔJ.